Reply to Reviewers – Smith et al., 2017

Comments - Editor

1. Your groundtruthing is not that solid. There is a well-established link between surface air temperatures and melt onset (e.g. Libo Wang et al. 2008, RSE) that you could investigate using surface climate observations. River flow data is another potential source of groundtruth information.

We have added an external validation section to the MS leveraging MODIS snow covered fraction (MOD10C1, Hall and Riggs, 2016) for assessing the end dates and High Asia Refined Analysis surface temperature (HAR - Surface Temperature, Maussion et al., 2014) for assessing the onset of melt. This is explained in more detail in specific reviewer comments below (General comments of reviewer 1, specific comment 2 of reviewer 2) as well as in the MS.

2. I suggest you make the study rationale a bit clearer in the Introduction e.g. the reason for monitoring snow melt duration. This is discussed in the Hydrologic Implications section, but it would be useful to make this clear at the beginning of the paper.

We have updated the introduction to expand on the rationale behind our study.

Comments – Reviewer 1

In this paper, the authors use passive microwave data to identify snowmelt onset, snowmelt end and snowmelt period over the High Mountain Asia (HMA) region. They verify the results of an automated algorithm by comparison to manually identified dates in the microwave signal and find it matches to within 5 days. They then use the algorithm to calculate the melt onset, end and period over 29 years and evaluate trends across the region. The paper is well written and provides a long-term record of snowmelt trends across a region where snowmelt is a critical source of water supply. They use an existing method for identifying melt, but apply new techniques for detecting onset and end, as well as a hierarchical clustering method to identify spatial patterns in the data. This paper contributes to the literature in an understudied area of
the world.

My main feedback is that the lack of validation data for this technique raises a number of questions. It would be useful to see validation of the approach in this region that would lend confidence to the results, independent of the microwave data. Some possible data sources that could be used include snow covered area from MODIS or VIIRS to estimate snowmelt end dates. Discharge data, if available, could be used to verify the onset of melt by evaluating the rising limb of the snowmelt hydrograph. Similarly, it may be possible to examine shifts towards earlier melt timing by looking at the hydrograph centroid. (See Regonda et al. 2004, Seasonal Cycle Shifts in Hydroclimatology over the Western United States, Journal of Climate, Vol. 18). Alternatively, temperature data may provide some verification of onset dates. If these data are not available, then demonstrating the approach in an area with data would be useful.

Thank you for the detailed comments and review. We agree that the lack of spatially and temporally extensive control data is a limitation of the study. Unfortunately, long-term, spatially extensive, and high-quality snow records are simply not available for the study region. In our revision, we leverage MODIS MOD10C fractional snow cover (Hall and Riggs, 2016) to assess the reliability of our snowmelt end dates, and High Asia Refined Analysis (HAR) modeled surface temperatures (Maussion et al., 2014) to examine our snowmelt onset dates.

We find that our snowmelt end dates agree very well (slope = 1.00, R^2 = 0.99, n=34,468 over 16 years) with the date of MODIS snow clearance (defined here as 5 out of 7 days below 5% snow-covered area). A comparison of MODIS and algorithm snow clearance dates is found below in Figure 1 of this reply. This figure and related discussion have been added to the manuscript in the Results section.

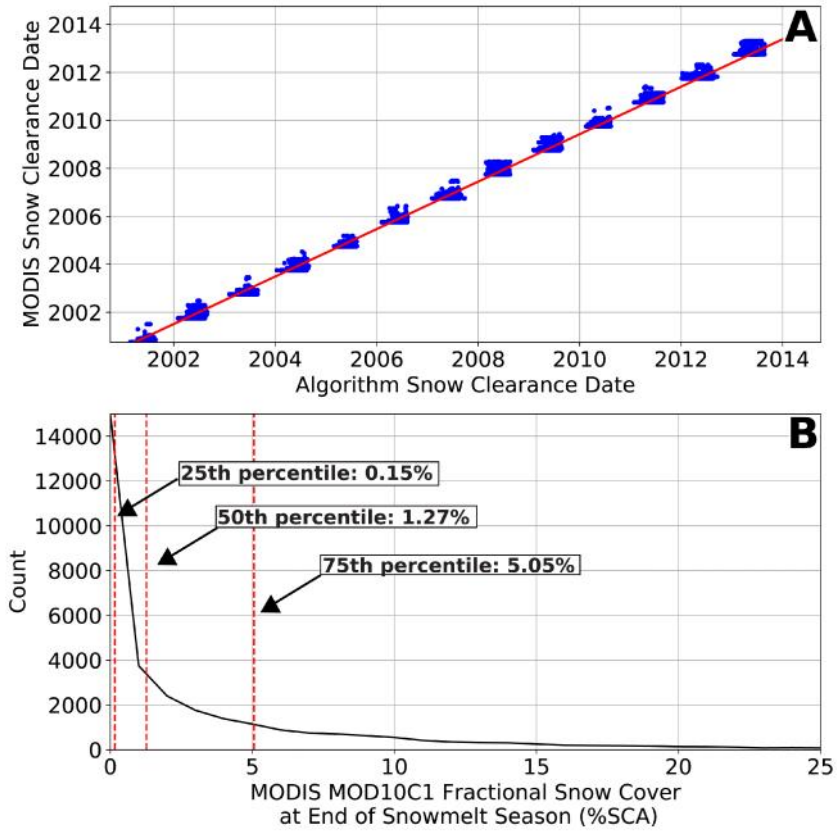

Figure 1 – Comparison of snowmelt clearance dates with MODIS MOD10C1. There is nearly 1-1 agreement between the chosen dates for snowmelt end (slope = 1.00, rsq =0.99, n=34,468). Nearly all algorithm-derived melt dates show less than 5% MODIS fractional snow cover, with nearly 50% showing less than 1% snow cover.

We only compare those dates where there is no cloud cover within 7 days of our algorithm-determined snowmelt end date to limit our analysis to only those years where both methods should provide equally accurate snowmelt end dates.

The accuracy of snowmelt onset dates is somewhat more complicated to determine. Snowmelt onset for this paper could be defined as either the first appearance of liquid water in the snowpack or the beginning of the primary 'melt-off' phase, where there are no more significant snowfall events detected in the passive microwave data and SWE generally starts to decline. In the original manuscript, we chose

simply the highest XPGR peak, which could correspond to either of these dates, depending on the climate – and particularly temperature – context of any given location. In this revision, we have updated the algorithm to flag years where there are multiple coherent peaks in the XPGR time series as being unreliable. These data points are no longer included in the trend analysis components of the paper to ensure that we only examine trends in reliably identified snowmelt dates. We find that ~25% of all snowmelt onset dates across all locations are flagged as unreliable, and thus we use 15% less data overall. Trend values are changed in some cases (cf. Fig 9 in the updated MS), mostly on the Tibetan Plateau where fewer trends are now statistically significant. A small area of the far eastern Tibetan Plateau shifts from slightly positive onset to slightly negative onset as well. Otherwise, the large-scale trend patterns are maintained. A more detailed discussion of this update is given below in response to reviewer 2 - Comment #3, as well as in Figure 2 of this reply.

General comments:

1. The 36 GHz signal saturates out in deep snow, which I expect much of this area experiences. How does that affect the gradient ratio approach, since the difference may remain fairly constant for much of the season? How do you know you're selecting the actual maximum XPGR?

Signal saturation is a problem in HMA and elsewhere – particularly in mountainous regions – and dramatically reduces the reliability of SWE estimates. However, even with signal saturation, the appearance of liquid water in the snowpack will cause 'spikes' in the XGPR signal due to the drastic difference between the passive microwave signal response to dry snow (volume scattering of the bare-earth passive microwave signal inside the snowpack) and wet snow (emission of passive microwave signal from the water layer). Our algorithm is sensitive to these spikes and we thus argue that it identifies snowmelt, even in cases where saturation may occur.

2. Related to question 1, the XPGR seems to follow the calculated SWE signal. How does the calculated SWE compare to general estimates of SWE in the region? Is it reasonable, or is there evidence of signal saturation?

Unfortunately, in-situ estimates of SWE in the region are sparse. Previous work has reported reasonable results for Western China (Che et al. 2008), but SWE estimates in complex and deep-snow terrain are generally considered unreliable (Tedesco et al., 2015). Without reliable in-situ estimations it is hard to quantify the degree of SWE underestimation due to saturation, but comparisons to modeled results (WRF, HAR) indicate that SWE is underestimated in HMA in some areas.

We aim to exploit shifts native to the time-series of each individual pixel instead of using absolute thresholds for tracking melt, as has been done in previous studies (e.g., Abdalati et al. 1995, Monahan and Ramage, 2010), so the reliability of absolute SWE measurements should not have an outsized impact upon our algorithm.

3. It is interesting that some of the trends change after 2002, when several additional instruments begin to be available and are included in the analysis. Is it possible that differences in the sensors are causing different results?

While it is possible that the differences in the sensors could have impacted the results, we think this is unlikely, as we explicitly designed the algorithm to be sensor-independent. First, our results rely on the XPGR, which is a normalized ratio and which should mitigate some, if not all, of the sensor-related differences between instruments. Second, we examine peaks native to each single-instrument time series, so detected melt onset and end dates are native to each instrument. Third, and most importantly, when there are multiple instruments providing a melt date for a given year, we use a conservative strategy for choosing a single melt onset/end date for each year.

For melt onset, if the time series has multiple coherent peaks (defined as two peaks within 5% of each other more than 3 weeks apart, the year is flagged as unreliable for melt onset determination (~25% of the total number of melt onset dates across all locations and years are flagged as such, with a few regions). If two instruments are providing a melt date, and they are less than two weeks apart, we choose the earliest date between the two. If there are three melt onset dates, we choose the median onset date. If the melt onset dates are more than two weeks apart, we flag the year as unreliable. We then use a similar strategy for the end of the melt season, which is generally better constrained by our algorithm. The only difference between the strategy for melt onset and melt end is when there are two end dates more than two weeks apart, we choose the date that is closest to the long-term average melt end date instead of flagging that year as unreliable.

4. Following on question 3, in section 2.3 the method used to merge the datasets for the hierarchical clustering analysis is described. Was this merged dataset also used in the snowmelt tracking analysis? If not, then explain why differences in the sensors wouldn't impact the estimated melt onset and end dates. If yes then this description should be included earlier.

The merged dataset was not used for the snowmelt tracking analysis to limit the impact of inter-sensor differences on the determination of melt onset and end. Merging the multiple passive microwave datasets introduces noise to the time series, which in turn impacts placement and magnitude of the peaks used to determine melt onset. We instead used the strategy described in reply to comment #3 above to choose the melt dates for years with multiple sensors. We only use the merged dataset for (1) display purposes on figures in the manuscript, and (2) for the hierarchical clustering. We chose to use the merged dataset for the hierarchical clustering to extend the time period we cluster over and to include data from each sensor to increase our cluster robustness throughout the entire study time period, despite the increase in noise from using multiple merged time series.

5. The manual selection of dates based on the time series seems subjective. It would be useful to include additional information on how those dates were selected. For example in Figure 3 – in both 2009 and in 2010 there were two peaks of similar magnitude during the winter season. In 2009 the one closer to the end of the season was selected despite appearing less than the earlier one. In 2010 the one very early in the season was selected despite there being an almost equal peak later on. The description in section 3.1 should be clearer.

We examined not only the XPGR, but the SWE and Tb37V signal at each year to determine snowmelt onset. Both 2009 and 2010 are complex cases, where there are multiple strong candidates for the onset of snowmelt. In 2009, the higher SWE total in the earlier peak, followed by a decreasing by oscillating SWE total, pointed to the earlier XPGR peak as the onset of melt. In 2010, the generally decreasing SWE

total throughout the winter, punctuated one large event and then a return to the previous decreasing curve a few weeks later indicated that the main snowmelt season started earlier. However, in both cases it could be argued that either peak represents the true start of the snowmelt season.

Please see the reply to comment #3 above about changes in the algorithm related to flagging poorly constrained years. Our updated comparison of our algorithm dataset and our control dataset does not include comparison of these poorly constrained melt onset dates. These dates are also no longer used in the assessment of snowmelt trends.

Specific comments:

1. Page 3, Line 25: why was this algorithm chosen over the other methods referenced in the introduction?

We choose this method due to (1) simplicity, (2) speed of calculation, and (3) lack of reliance on pre-calculated metrics or assumptions. For example, diurnal temperature algorithms rely on fixed differences between day and night temperatures to detect melt; these differences are neither constant in space nor in time (intra- and inter-seasonal) across our large and diverse study area. We found that the XPGR algorithm was well-suited to the time series approach we use, and was fast enough to compute for the entire dataset we used. It has the additional advantage of only relying on night-time data, which somewhat limits the impact of sporadic daytime melt (due to solar radiation) on our results.

2. Section 2.1: additional background information on passive microwave detection of snow and snowmelt is needed, specifically on how the signal is affected by liquid water in the snow at different frequencies.

Section 2.1 (Section 2.2 in the new MS) has been updated with additional information on the interactions of snow and passive microwave radiation.

3. Page 4, Line 7: Was SWE calculated using the Chang algorithm on Tb from the different sensors? Or are you using the SWE products developed for the different sensors? Adding the equation would be useful. How do you combine multiple sensors when available?

We use the original Chang algorithm for each sensor, albeit tuned to each sensor (i.e., the Chang algorithm is offset by 5K when the AMSR-E frequencies are used). As our algorithm relies primarily on the normalized XPGR index and we do not aim to provide a tightly-constrained SWE product, we leverage a single, consistent algorithm across all satellite datasets. We have added the equation to the MS in Section 2.1. We combine the SWE datasets for display purposes (e.g., Figure 3 of the MS) by resampling a combined, multi-instrument, timeseries to the daily mean SWE value.

4. Page 5, line 2: Not sure what is meant by "regularize".

We perform a simple linear regression of the overlapping pieces of the time series to determine the offset between the overlapping datasets. We then add or subtract the determined coefficients to bring

the time series closer to a single coherent dataset (cf. Figure 2 of the MS) in order to use the longest possible time frame for our hierarchical clustering. We have clarified this in-text.

5. Page 5, lines 23-25: How does the standard deviation of the melt onset date vary spatially? It seems this approach would work best in high elevation/deep snow regions, whereas along the edges in lower elevation where the snow is more ephemeral there might be more error. This would also affect estimates of melt period.

Very true. However, we find that the highest deviation regions are those areas where deep snow impacts the algorithm, or late-season storms change the snowmelt onset date from year-to-year. Ephemeral snowmelt is actually tracked quite well, as it tends to have sharp peaks and a single, continuous melt-off curve. Those areas where snow varies significantly year-to-year, and areas with multiple SWE peaks, are more difficult (ie, in the Karakoram, cf. Fig 2 of this reply and Figure S5 in the revised manuscript). We have attempted to reduce this error by flagging unreliable years in our melt dataset as described above. A map of the standard deviation of melt onset dates for 29 years has also been added to the Supplement (Figure S5). Note that many low-STD regions are areas where there is almost no snow (e.g., Tarim Basin and low-elevation areas of the Himalayan front). These areas are not included in our trend analysis.

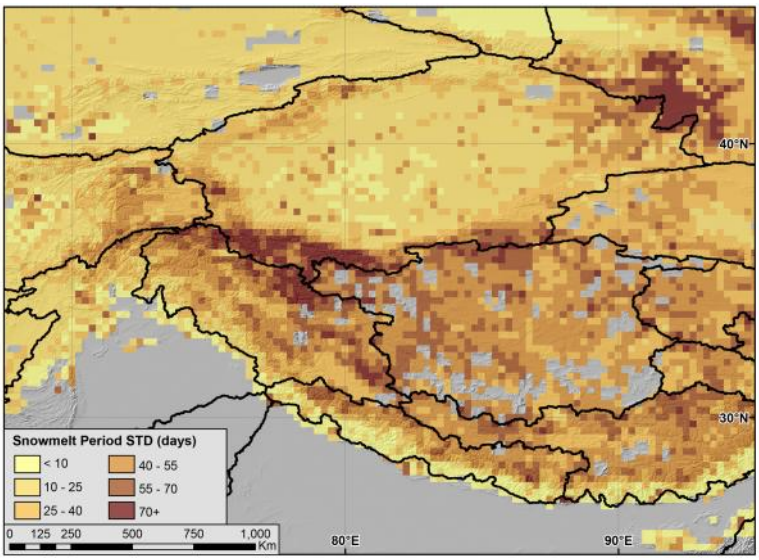

Figure 2 – Standard deviation in snowmelt period, calculated over the full 29-year dataset. Low standard deviation areas follow low-SWE and low-elevation zones, with more variable snowfall regions (ie, Karakoram) showing higher standard deviations.

6. Page 6, line 8: Where you say, "snow is present for less than a month on average." Are you referring to the snowmelt period or the entire snow season? That sounds like the entire season, but everywhere else is referring to melt period.

You're correct, we refer here to short snowmelt periods. We remove data that have a long-term average snowmelt period of less than 20 days. We have updated the wording in the MS.

7. Page 6, line 24: You say, "As can be seen in Figure 3, inter-annual variation in snowfall can cause large disparities in the yearly dates of snowmelt onset and end." Based on Figure 3 there doesn't appear to be a lot of variability – the peak SWE is around 100mm each year. Are you referring to timing of snowfall events?

Yes, we refer here to the timing and magnitude of SWE buildup and melt. Each year has quite different peak locations, and relative peak sizes. This has been clarified in the MS.

8. Figure 1. Can you identify on the overview map the location of the sample data shown in figures 2 and 3?

This has been updated.

9. Figure 4: What do the gray areas on the plateau represent? Provide an explanation, similar to figure 6.

This has been updated.

Comments – Reviewer 2

Passive microwave satellite data have been used for snowmelt onset detection on nearly all components of the cryosphere (e.g. ice sheets, sea ice, lake ice, and seasonal snow cover) mainly at the northern middle to high latitudes and Antarctica, where there is permanent or relatively stable snow accumulation each winter. It has also been used to classify daily freeze/thaw state dynamics for global vegetated land cover regions without distinguishing individual elements of the landscape (e.g. soil, vegetation, snow). The current study detects snowmelt onset/end dates and snowmelt season in Tibetan Plateau and its surrounding mountain ranges, and analyzes trends in snowmelt timing during the 1987-2016 period. Snowmelt onset detection is based on the crossed-polarized gradient ratio (XPGR) algorithm developed in previous studies, and the end of snowmelt is determined by time series of Tb37v and snow water equivalent (SWE) calculated using the Chang et al. (1987) algorithm. It is a useful extension to previous studies. However, there are several caveats in the method used for snowmelt onset/end detection in this study as described below.

Specific Comments

First of all, there are no in situ observations used for either thresholds calibration or results validation. I wonder how the authors know the selected thresholds are associated with the actual snowmelt onset/end? Although a manual control dataset was generated and used for results evaluation, the control dataset was produced subjectively from the interpretation of the satellite data only.

In the updated manuscript we have added a section comparing our results to MODIS snow cover and HAR mean daily surface temperature (see also reply to comment #1 of reviewer 1, and the extended discussion of comparison to control datasets in response to your comment below). In situ data at the correct spatial and temporal scale simply does not exist for the majority of the study region, so we rely on these proxies instead. An updated discussion of the caveats of the method and uncertainties is included in the MS.

The annual peak value of XPGR was used to identify snowmelt onset, which appears to correspond to dates of annual maximum SWE and very low Tb37v (Fig.3). Fig.3 shows that the brightness temperatures at 37GHz are <= 225K on the detected snowmelt onset dates for three out of the four winters. From my experience, the snowpack is unlikely to be melting under such low brightness temperatures. The magnitude of Tb37v was used as a condition for snowmelt detection in some previous studies, but it was always >= 248K.

Thank you for this important critique. We have modified our algorithm as described in comment #3 of reviewer #1. In addition to this, we have compared our melt onset dates to both MODIS fractional snow-covered area and HAR modeled surface temperature. Figure 3 below shows the HAR surface temperature distribution at melt onset. While average daily temperatures tend to be negative, daytime temperatures are often positive (average 4C), with large (20+ degree) temperature variation. Figure 4 below shows a direct comparison between our melt onset dates and the MODIS and HAR datasets. As can be seen in the middle panel, the onset of melt correlates with the peak of MODIS fractional snow cover, and with the yearly minimum temperature from HAR (this has been added to the Supplement as Figure S2). This implies that our melt algorithm is capturing the turning point where snow ceases to increase and starts melting out. These figures have been added to the Supplement.

We also compared HAR air temperature to the raw Brightness Temperature (Tb) values (Figures 5 and 6 of this reply and S3-4 in the updated Supplement), and found that while there is a definite correlation between air temperature and Tb, positive surface temperatures are associated with a wide range of possible Tb values. The Tb-Temperature distribution is also quite different between spatial locations, implying that a single threshold would not be appropriate for determining the possibility of snowmelt from Tb values.

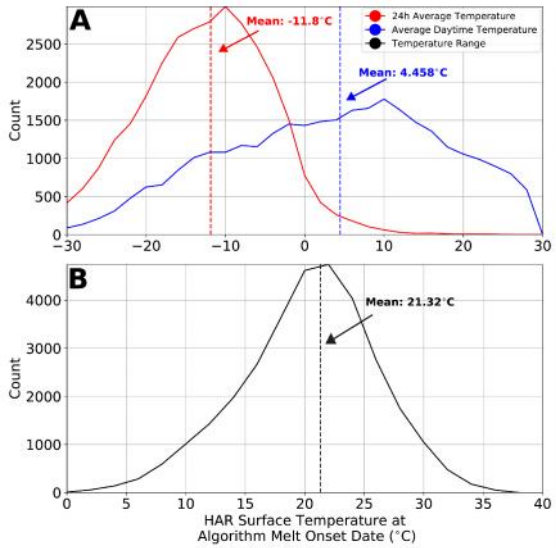

Figure 3 – HAR modeled hourly surface temperature (Maussion et al., 2014) at the date of algorithm-melt onset. Average daily temperature (red) and average daytime temperature (blue) show divergent means, where the onset of melt is characterized by below zero average temperatures, but daytime temperatures that are positive. The average daily range of temperatures (black) shows quite large variability in 24h temperature profile at the onset of snowmelt.

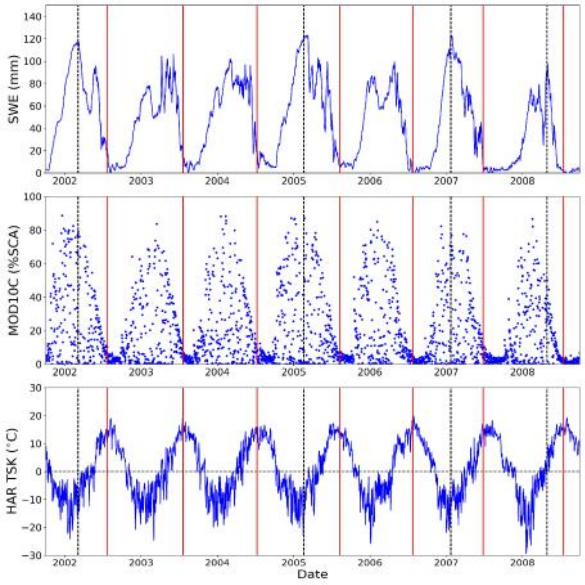

Figure 4 – Representative sample point showing SWE (top, this study), MODIS fractional snow covered area (middle, Hall and Riggs, 2016), and HAR daily average temperature (bottom, Maussion et al., 2014) over the period 2001-2009. Algorithm-derived melt onset dates (dashed lines, black) and end dates (solid lines, red). Years with multi-peaked XPGR data do not return a melt onset date. Melt onset dates correlate well with peak annual snow-covered area (middle) and the yearly minimum temperature (bottom), implying that our melt algorithm captures the onset of the snowmelt season accurately. Data taken from 71.25E, 36.75N.

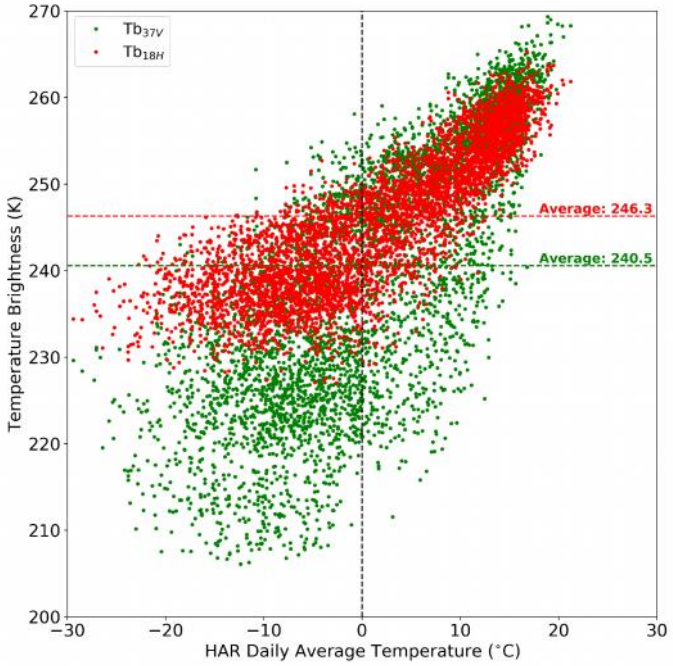

Figure 5 – HAR Average daily temperature vs Temperature Brightness (37V in green, 18H in red). Both channels show correlations with air temperature, but show a wide spread. This observation indicates that there is no single Temperature Brightness threshold that can be used for snowmelt detection.

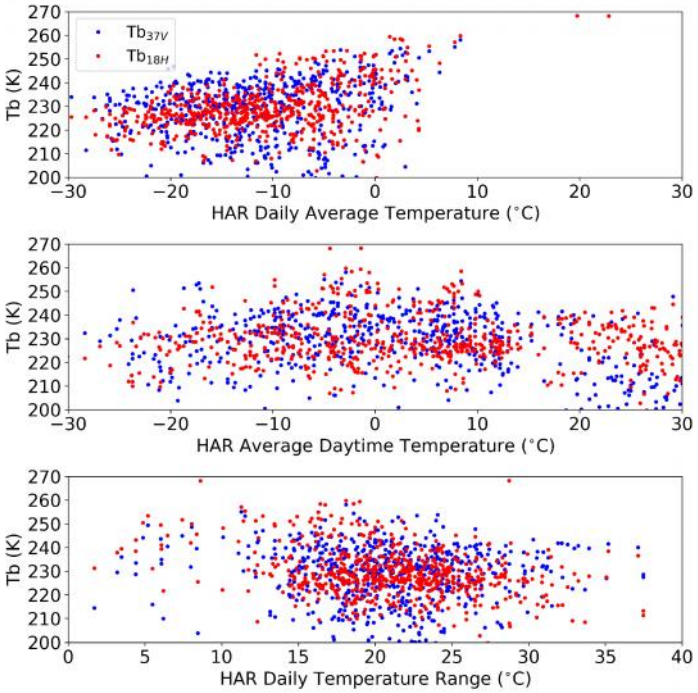

Figure 6 – HAR temperature metrics vs Tb at snowmelt onset. Both 37V (blue) and 18H (red) channels show significant spread. While there is a slight correlation between average daily temperature and Tb, average daytime temperature is very poorly related to Tb. This implies that the night-time passive microwave data we use to track snowmelt onset still captures the impacts of above-zero daytime temperatures.

The XPGR algorithm was developed and used for melt detection on the Greenland ice sheet. Several studies have shown that the XPGR technique detects less melt extent and duration than other algorithms (e.g. Ashcroft and Long, 2006; Fettweis et al., 2006). Ascraft and Long (2006) compared six different melt detection methods using either active or passive microwave satellite data over the Greenland ice sheet for the year 2000, including the XPGR method. They found that compared to other methods, XPGR detected significant less melt extent and duration on Greenland (see Table 2 from their paper). Therefore, in my opinion the XPGR method is not suitable for snowmelt detection, especially without proper calibration/validation.

In our usage of the XPGR, we do not rely on static melt thresholds, as has been done in the original Abdalati and Steffen (1995) study and the studies of Fettweis et al. (2006) and Ashcroft and Long (2006). Ashcroft and Long (2006) note that "with XPGR, local maxima in q(t) occur at times similar to those observed for the a-based and Tb-M methods; however, the relative amplitude of the peaks are different, contributing to discrepancies in the melt detection by XPGR and the other methods." This implies that the timing of melt events is detected in the XPGR time series, but the use of a single threshold calculated for all of Greenland negatively impacts melt detection. High elevation and internal areas are classified with the same cutoff as low elevation and coastal areas in their study. In our method, we do not rely on a single cutoff, but instead find the XPGR peak unique to individual years and locations.

It should also be noted that we do not classify individual days as melting or not melting, as has been done in the previously mentioned studies, but instead seek to identify the primary start and end dates of the snowmelt season. Ashcroft and Long (2006) further note "the differences in the melt detected by the individual methods are attributed to differences in sensitivity to melt due to frequency and/or differences in the definition of melt implicit with each method." Based on our stated goal of identifying the primary melt period, and the data comparisons presented in Figures 1-6 of this reply, we maintain that the XPGR is a useful metric.

"To determine the end of the snowmelt season, we choose either the date of the yearly maximum Tb37V value, which corresponds to the thinnest snowpack or to a 'bare earth' signal, or the first date where 4 out of 5 days have been within 2 cm of the yearly SWE minimum." SWE calculated using the Chang et al. (1987) algorithm was used for snowmelt end detection in this study. However, the Chang et al. (1987) algorithm was found to overestimate SWE or snow depth in western China (Chang and others, 1992; Che et al., 2008). SWE retrieval from passive microwave data is based on volume scattering of the microwave signals by snow, thus SWE can't be estimated accurately when the snowpack is wet. Most SWE retrieval algorithms are only applied to data from the morning orbit to mitigate the impact of wet snow. The snowpack is likely to be wet and shallow near the end of snowmelt, which would lead to erroneous SWE retrievals from the passive microwave data. Wang et al. (2013) showed that it was a challenge to discriminate wet snow from snow-free land using satellite data alone.

We realize the shortcomings of the Chang algorithm, particularly for wet snow depth estimation at the end of the snowmelt season. This is why we do not simply identify snow clearance as days where SWE reaches zero, but allow the algorithm to declare the end of the melt season when small amounts of SWE remain, or when Tb37 has reached its yearly max. In our now included validation with MOD10C, we find very close agreement between our melt end dates and the MOD10C snow fraction dropping below 5% for five out of seven consecutive cloud-free days (Figure 1 of this reply, Figure 4 in the updated MS). We thus argue that our method successfully identifies the end of the snowmelt season despite problems inherent with passive microwave SWE estimation.

The estimated mean snowmelt periods in the current study are nearly 150 days for large areas of Tibetan Plateau during the 1987-2016 period (Fig.4), while Ke et al. (2016) showed that the annual mean snow cover days were 120 days during the 1981/82 – 2009/10 period based on observations from weather stations (see their Fig.3). This suggests that the detected snowmelt end dates in the current study are likely too late (Fig.5). On account of the above, I recommend rejection of the paper.

The reviewer raises an important point that we address with the following four comments:

(1) The cited Ke et al. (2016) study uses local station data to estimate the length of the snow-cover season for Western China. However, from their Figure 1, their station density is very poor, particularly in the Tibetan interior. Their following Figure 3 (snow-covered days) seems to be interpolated from these sparse points, which may or may not be representative of the large, unmonitored areas. Additionally, other studies of snowcover in Tibet (e.g., Pu et al., 2007) note extensive areas of 9+ month snow cover using MODIS data (their Figure 4).

    The coherence between independent snow-clearance measures (Figure 1 of this reply, MODIS and Passive Microwave) leads us to argue for the reliability of our snowmelt clearance dates. The non-representative spatial and elevation distribution of weather stations in the Ke et al. (2016) study, along with difficulties of scaling up snow measurements at point locations and interpolating them over diverse terrain, could account for some of the difference between the results of the two studies.

(2) As snowmelt period depends on two measurements (the onset and the end date), discrepancies between our snowmelt periods and those shown in Ke et al. (2016) are more likely to come from mismatches in the snowmelt onset date. However, as is shown in Figures 2 and 3 of this reply, our melt onset dates generally track the start of the upward arm of the yearly temperature distribution, and are correlated with dates of positive daytime surface temperatures.

(3) In order to examine the reviewer's comments about snowmelt period in more detail, we tested an additional change to the melt tracking algorithm with an imposed Tb threshold on the onset date of melt (after Fettweis et al., 2006). This threshold was chosen so that snowmelt was only found if the Tb18H was above the long-term average Tb18H plus one half standard deviation. This method was used previously in Greenland to improve the XPGR method with the stated goal of flagging each day of the year as melting or not melting.

    We find that this dramatically reduces snowmelt periods (Fig. 7 of this reply, below), but also reduces the agreement between our algorithm data and the MODIS and HAR control datasets. Onset dates correlate with quite low (~10%) snow fraction, and with positive (+15C) average daily temperatures. Melt periods in regions outside of the Tibetan Plateau shrink significantly, and no longer match up with other published literature. This implies that by imposing this threshold, we examine only the very end of the snowmelt season, and not the true onset of snowmelt.

    Importantly, we also compared trends in our data using both methods (adaptive XPGR threshold and with the addition of a fixed Tb threshold) and found that most regions maintained the same trend direction, if not trend magnitude. Thus, trends in melt end date and melt period are similar between both methods. The largest discrepancy is in the far eastern Tibetan Plateau, where melt onset trends shift from negative to positive when the fixed thresholding method is

used. The northern regions of HMA (north of the Tien Shan) also do not exhibit statistically significant trends for all three metrics (onset, end, period). We attribute these differences to the fact that the two methods are really tracking two separate measures of snowmelt onset. In our method (which is used and described in the MS), we track the turning point of the yearly temperature cycle and the peak time when snow first starts to decrease. Using the threshold metric, we track the last strong pulse of snowmelt, when much of the snow has already melted or sublimated away. For these reasons, we maintain that our algorithm, with the changes described here in this reply and in the updated MS, is a valid way to track the snowmelt in this context.

(4) Lastly, we argue that the context for the previously cited snowmelt studies and this study are different. Most of the snowmelt algorithms have been developed over Greenland or for tracking sea ice. As the altitudes and latitudes of these study locations are drastically different, solar radiative forcing is generally larger in High Mountain Asia. Additionally, we modify the static approach used in previous algorithms to derive snowmelt over a wide range of topographies, and thus the efficacy of the previous snowmelt algorithms and our algorithm cannot be directly compared.

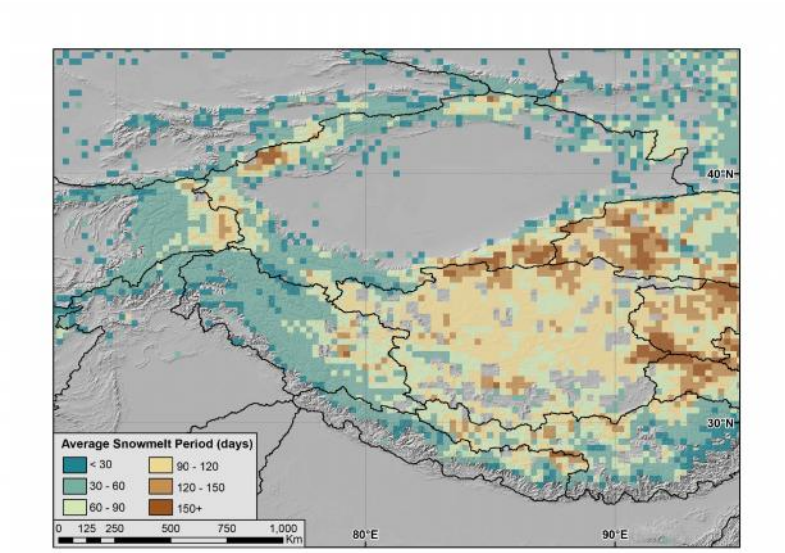

Figure 7 – Average snowmelt period when a more conservative Tb18H threshold is applied to the method. While melt periods in Tibet match better with those proposed in Ke et al. (2016), melt periods in the western regions of HMA are unreasonably low.

We argue that despite the shortcomings of passive microwave data – and the lack of large-scale ground control data – our algorithm accurately tracks the onset and end of the snowmelt season. An updated discussion of methods, caveats, and comparisons to the control datasets have been added throughout the manuscript.

References

Abdalati, W. and Steffen, K.: Passive microwave-derived snow melt regions on the Greenland Ice Sheet, Geophysical Research Letters, 22, 787–790, 1995.

Che, T., Xin, L., Jin, R., Armstrong, R., and Zhang, T.: Snow depth derived from passive microwave remote-sensing data in China, Annals of Glaciology, 49, 145–154, 2008.

Fettweis, X.; Gallee, H.; Lefebre, F.; van Ypersele, J. P. The 1988-2003 Greenland ice sheet melt extent using passive microwave satellite data and a regional climate model. Climate Dynamics. 2006, 27 (5): 531-541.

Hall, D. K. and G. A. Riggs. 2016. MODIS/Terra Snow Cover Daily L3 Global 0.05Deg CMG, Version 6. Boulder, Colorado USA. NASA National Snow and Ice Data Center Distributed Active Archive Center. doi: http://dx.doi.org/10.5067/MODIS/MOD10C1.006. 27.6.2017.

Ke et al., 2016, Variability in snow cover phenology in China from 1952 to 2010, Hydrol. Earth Syst. Sci., 20, 755–770, doi: 10.5194/hess-20-755-2016.

Maussion, F., D. Scherer, T. Mölg, E. Collier, J. Curio, and R. Finkelnburg: Precipitation seasonality and variability over the Tibetan Plateau as resolved by the High Asia Reanalysis, J. Climate, 27, 1910-1927, doi:10.1175/JCLI-D-13-00282.1, 2014.

Monahan, P. A. and Ramage, J.: AMSR-E melt patterns on the Southern Patagonia Icefield, Journal of Glaciology, 56, 699–708, 2010.

Pu, Zhaoxia, Li Xu, and Vincent V. Salomonson. "MODIS/Terra observed seasonal variations of snow cover over the Tibetan Plateau." *Geophysical Research Letters* 34.6 (2007).

Tedesco, M., Derksen, C., Deems, J. S., and Foster, J. L.: Remote sensing of snow depth and snow water equivalent, Remote Sensing of the Cryosphere, pp. 73–98, 2015.

Wang, L., Derksen, C., and Brown, R., and Markus, T., 2013, Recent changes in pan-Arctic melt onset from satellite passive microwave measurements, Geophys. Res. Lett., 40, 522–528, doi:10.1002/grl.50098.

Spatio-temporal Patterns of High Mountain Asia's Snowmelt Season Identified with an Automated Snowmelt Detection Algorithm, 1987-2016

Taylor Smith[1], Bodo Bookhagen[1], and Aljoscha Rheinwalt[1]

[1]Institute for Earth and Environmental Sciences, Universität Potsdam, Germany

Correspondence to: Taylor Smith (tasmith@uni-potsdam.de)

Abstract. High Mountain Asia (HMA) ~~,~~ – encompassing the Tibetan Plateau and surrounding mountain ranges ~~,~~ – is the primary water ~~tower~~ source for much of Asia, serving more than a billion downstream users. Many catchments receive the majority of their yearly water budget in the form of snow, which is poorly monitored by sparse in-situ weather networks. Both the timing and volume of snowmelt play critical roles in downstream water provision, as many applications – such as agriculture, drinking-water generation, and hydropower – rely on consistent and predictable snowmelt runoff. Here, we leverage passive microwave data across five sensors (SSMI, SSMIS, AMSR-E, AMSR2, and GPM) from 1987-2016 to track the onset and end of snowmelt across HMA. ~~Compared against a~~ We validated our method against climate-model surface temperatures, snow-cover data, and a manual control dataset (n=2100, 3 variables at 25 locations over 28 years)~~,~~; our algorithm is generally accurate within 3-5 days of the onset and end dates of melt. Using the algorithm-generated snowmelt dates, we examine the spatiotemporal patterns of the snowmelt season across HMA. The climatically short (29 year) time series, along with complex inter-annual snowfall variations, makes determining trends in melt onset and end dates at a single point difficult. We instead identify trends in snowmelt timing by using hierarchical clustering of the passive microwave data to determine trends in self-similar regions. We make the following four key observations: (1) The end of the snowmelt season is trending almost universally earlier in HMA (negative trends). Changes in the end of the snowmelt season are generally between 2 and 8 days/decade over the 29-year study period (5 - 25 days total). The length of the snowmelt season is thus shrinking in many, though not all, regions of HMA. Some areas exhibit later snowmelt onset dates (positive trends), but with a generally smaller magnitudes than trends in snowmelt end. (2) Areas with long snowmelt periods, such as the Tibetan Plateau, show the strongest compression of the snowmelt season (negative trends). These trends are apparent regardless of the time period over which the regression is performed. (3) While trends averaged over three decades indicate earlier snowmelt onset and end, data from the last 14 years (2002-2016) exhibit positive trends in both snowmelt onset and end dates in many regions, such as parts of the Pamir and Kunlun Shan. Due to the short nature of the time series, it is not clear whether this change is a reversal in a long-term trend or simply inter-annual variability. (4) Some regions with stable or growing glaciers – such as the Karakoram and Kunlun Shan – see slightly later snowmelt onset and longer snowmelt periods. It is likely that changes in the snowmelt regime of HMA account for some of the observed heterogeneity in glacier response to climate change. While the decadal increases in regional temperature have in general caused earlier snowmelt onset and shortened melt seasons, changes in HMA's crysophere have

been spatially and temporally heterogeneous. The complex response of HMA's cryosphere to climate change highlights the importance of both regional and small-scale studies for effective water planning.

1 Introduction

More than a billion people across Asia rely directly or indirectly on water sourced from melting snow in High Mountain Asia (HMA) (Bookhagen and Burbank, 2010; Bolch et al., 2012; Kääb et al., 2012; Kang et al., 2010; Immerzeel et al., 2010; Gardner et al., 2013; Hewitt, 2005; Malik et al., 2016). Many catchments receive the majority of their yearly water budget in the form of snow – particularly at high elevations (Barnett et al., 2005). Both the volume of snowfall and the timing of snowmelt play crucial roles in the efficacy of water provision for downstream users, as many applications – such as agriculture and hydropower – rely on consistent and predictable water availability. Many areas also rely on snowmelt to provide a water buffer late in the year ~~,~~ when direct precipitation is rare. Any changes in the onset, length, or intensity of the snowmelt season will impact the water security of both high-elevation and downstream communities.

Passive microwave (PM) data has been used to estimate snow depth and snow-water equivalent (SWE) since the launch of the Scanning Multichannel Microwave Radiometer (SMMR) in 1978. Consistent, pseudo-daily measurements became available in 1987 with the launch of the Special Sensor Microwave/Imager (SSMI) series of sensors (Wentz, 2013). PM data is highly sensitive to liquid water present in the snowpack, and is thus a valuable tool for tracking the onset of snowmelt across large, inhospitable, and unmonitored regions. PM data also have the advantage of functioning despite cloud cover, which is ubiquitous in much of HMA during ~~the~~ both winter and during the Indian Summer Monsoon (ISM) season. Using satellite-derived PM measurements, several authors have tracked the onset, duration, and spatial extent of snowmelt events using a range of approaches including the cross-polarized gradient ratio (XPGR) (Abdalati and Steffen, 1995; Hall et al., 2004), the advanced horizontal range algorithm (Drobot and Anderson, 2001), Gaussian edge detection (Joshi et al., 2001), channel differences (Takala et al., 2003), artificial neural networks (Takala et al., 2008, 2009), diurnal temperature brightness (Tb) variations (Apgar et al., 2007; Monahan and Ramage, 2010; Tedesco, 2007), and wavelet-based approaches (Liu et al., 2005).

In this study, we adapted a previously published algorithm (Abdalati and Steffen, 1995) ~~, which~~ that relied on the establishment of a single cutoff threshold for identifying melt phases ~~,~~ to the more complex and diverse snow regimes of HMA. While previous studies have successfully measured snowmelt in large, homogeneous environments such as Greenland and Antarctica, we found these algorithms ineffective in the highly variable topography and snow dynamics of HMA. Here ~~,~~ we present an enhanced and generalized snowmelt algorithm building on previous work to improve on snowmelt detection in HMA. We then apply this algorithm to PM data from 1987-2016, and use the derived melt start and end dates to examine spatio-temporal snowmelt patterns across the entire HMA region.

1.1 Geographic Setting

HMA is comprised of several mountain ranges – the Himalaya, Pamir, Karakoram, Hindu Kush, Tien Shan, and Kunlun Shan – which contain the headwaters of major watersheds which serve more than a dozen countries (Fig. 1). Many of these catchments,

such as the Tibetan Plateau, Tarim, Syr Darya, Amu Darya, and Indus, rely on snowmelt for more than 50% of their yearly water budget (Bookhagen and Burbank, 2010; Shrestha et al., 2015). Many communities – particularly those at high elevations or those that depend on surface water for agriculture – are highly reliant on the timing of snowmelt. An early snowmelt season can create a late-season 'water gap' when a dry spell is caused by snow meltwaters disappearing before the start of the next rainy season. These water gaps can also negatively impact flora and fauna which depend heavily on the timing of the appearance of ephemeral water bodies (Bookhagen, 2017). The timing and volume of snowmelt thus has important implications for the environment, direct household water use, agriculture, and hydropower.

Several interacting moisture sources, ~~such as~~ including the Winter Westerly Disturbances (WWD), Indian Summer Monsoon (ISM), and East Asian Summer Monsoon (EASM), are responsible for the wide range of snowfall regimes across HMA (Fig. 1, inset). The interaction of these climatic regimes with the complex topography of HMA – particularly the vast elevation gradients – creates a diverse set of snowfall regimes (Cannon et al., 2014; Kääb et al., 2012; Immerzeel and Bierkens, 2012; Gardner et al., 2013; Kapnick et al., 2014; Barnett et al., 2005; Dahe et al., 2006; Takala et al., 2011; Cannon et al., 2017).

2 Materials and Methods

2.1 Datasets

We leverage a combined time series of SSMI (1987-2009), Special Sensor Microwave Imager/Sounder (SSMIS) (2008-2016), Advanced Microwave Scanning Radiometer - Earth Observing System (AMSR-E, 2002-2011), AMSR2 (2012-2016), and Global Precipitation Measurement (GPM, 2014-2016) data, processed to 0.25 decimal degree (dd) resolution by interpolating raw PM swath data at a series of point locations as described in Smith and Bookhagen (2016) (see Supplementary Table ~~1~~ S1 for a full dataset listing). In essence, we group all measurements within a 0.125° dd radius of each point on a 0.25° dd grid and generate a spatially weighted mean value for each swath at that point. The dataset is comprised of 6,399 point locations, with on average 26,000 PM measurements each (long-term average of 2.4 measurements/day for 29 years, with more measurements during the 2002-2016 period).

PM measurements are converted to snow-water equivalent (SWE) using the Chang equation (Eq. 1) (Chang et al., 1987) , with modifications for non-SSMI platforms as proposed by Armstrong and Brodzik (2001) , and a constant snow density of 0.24 g/cm^3 as proposed by Takala et al. (2011) .

$$SD[cm] = 1.59[cm/K] * (Tb_{18V} - Tb_{36V})[K] \quad (1)$$

Studies have noted that SWE estimates from the Chang equation have high uncertainties (e.g., Kelly et al., 2003; Kelly, 2009; Tedesco an particularly in dense forests. However, as much of our study area is non-forested – and we use SWE only as a rough estimate of snow volume – we choose to rely on the simple Chang equation rather than a more complex algorithm for SWE estimation.

As control data, we analyze Moderate Resolution Imaging Spectroradiometer (MODIS) percentage snow-covered area (product MOD10C1 V6, 2001-2016, (K. and Riggs, 2016)) and High Asia Refined Analysis (HAR) surface temperature (tsk,

2000-2014, (Maussion et al., 2014)). While these datasets only cover a subset of our study period, they are among the few independent control datasets available across the entire study area.

2.2 Snowmelt Tracking Algorithm

The shift from dry snow, which can be physically characterized as snow crystals in an air background, to wet snow, which replaces the air matrix with water, shifts the primary interaction between PM radiation and the snowpack from volumetric (dry snow) to surface (wet snow) scattering. These scattering changes are reflected in the temperature brightness (Tb) data, and allow wet and dry snow to be differentiated, as the transition from dry to wet snow drastically increases the measured Tb – particularly in the scattering (Tb_{37V}) channel. The XPGR, as originally described by Abdalati and Steffen (1995), is defined as:

$$XPGR = (Tb_{19H} - Tb_{37V})/(Tb_{19H} + Tb_{37V}) \quad (2)$$

This algorithm takes advantage of both the channel difference between the Tb_{19} and Tb_{37} GHz channels as well as the depolarization effects of snowmelt, which increases the differences between the horizontally and vertically polarized channels (Abdalati and Steffen, 1995). As this algorithm is normalized, it does not require ground calibration data, which is advantageous in HMA. Snowmelt onset can be determined using either a static or dynamic threshold. In the original application of the XPGR on the Greenland Ice Sheet, a static value of -0.025 was used to detect snowmelt (Abdalati and Steffen, 1995).

We find that for the majority of HMA, the -0.025 threshold is much too low to effectively detect melt. Indeed, the yearly peak XPGR is highly variable throughout time and space, and a constant threshold was found to be inappropriate for HMA. Additionally, while the XPGR time series is effective for tracking the onset of snowmelt, it is not effective for tracking the cessation of snowmelt. To track the end of snowmelt, we leverage two additional datasets: (1) the raw Tb_{37V} time series, which rapidly increases as snowpack thins, and (2) a SWE time series calculated from the Tb_{19} and Tb_{37} GHz channels (Chang et al., 1987; Kelly et al., 2003; Tedesco et al., 2015; Smith and Bookhagen, 2016).

We first use a simple peak-finding algorithm, which identifies peaks as points which are larger than their two neighboring samples, to generate a list of potential peaks in the XPGR data. Next, we take the average XPGR value within $\pm$ ~~3~~ 2 days of each peak to determine not only the simple yearly maximum XPGR, but the highest and temporally widest peak in our XPGR data. We flag years which have multiple strong and temporally distinct XPGR peaks as unconstrained for snowmelt onset estimation, as the algorithm has trouble consistently identifying snowmelt onset in these cases.

To determine the end of the snowmelt season, we choose either the date of the yearly maximum Tb_{37V} value, which corresponds to the thinnest snowpack or to a 'bare earth' signal, or the first date where 4 out of 5 days have been within 2 cm of the yearly SWE minimum. We choose the yearly SWE minimum instead of zero as our SWE threshold for snow clearance because some regions in HMA have a defined melt season but rarely reach zero SWE. This also helps control for uncertainty in shallow SWE measurements, as detecting shallow snow (<5 cm) with PM data is still difficult (Kelly et al., 2003; Armstrong and Brodzik, 2001). A full description of our melt detection algorithm is available in the Supplement (~~Figure S1~~Figs. S1-4).

2.3 Manual Control Dataset Generation

Unfortunately, large-scale and several-decades long snowmelt onset and end date records are not available for HMA. Instead, we use HAR (Maussion et al., 2014) and MODIS (K. and Riggs, 2016) data alongside a manually generated set of control dates for the onset and end of snowmelt, determined from the SWE, XPGR, and Tb_{37V} signals by the researchers. We visually identified major peaks, as well as the cessation of snowmelt, by inspection of the time series. We chose a random sample of 25 point locations across our study area, and identify start and end dates for each year of the time series (n=1400). We use the calculated length of the snowmelt period as an additional control variable (n=700).

2.4 Hierarchical Clustering

Hierarchical clustering is a method used to correlate time series data by intrinsic similarity (Corpet, 1988; Johnson, 1967; Jain et al., 1999; Murtagh and Contreras, 2012; Rheinwalt et al., 2015), which has been used extensively in the environmental research community. We generate clusters from those time series which share the most temporal overlap, or where the periodicity of Tb values have the largest coherence, regardless of their spatial correlation.

We choose the XPGR time series as our clustering variable, as the XPGR is the most sensitive to melt dynamics, integrates multiple Tb frequencies, and is not sensitive to SWE calibration issues. To improve the robustness of our clustering, we combine the disparate single-instrument PM time series into a single coherent time series which leverages the full temporal extent of each dataset (1987-2016), using the following three steps: (1) We standardize the PM signals of the suite of instruments used in this study to a single set of dates, artificially created at daily resolution from the minimum and maximum dates across all satellite datasets, by resampling all individual satellite time series to a daily time step and dropping dates without data. (2) We ~~regularize~~ homogenize the disparate PM time series based on the overlapping portions of individual satellite time series, using linear regression. The results of these regressions can be seen in ~~Table S2~~Tables S2-5, with an example regression at a single point shown in Figure 2. (3) In order to reduce noise in our cluster analysis, we resample our merged XPGR time series to a 5-day temporal resolution (pentad).

Next, we normalize each merged pentad time series (1987-2016) to a Gaussian distribution, using a percentile mapping approach (Rheinwalt, 2017). We then estimate the Pearson correlation coefficient to classify regions of self-similarity in our XPGR time series (Rheinwalt, 2016). This method computes a Pearson correlation coefficient between each time series, and based on the resulting correlation matrix, computes a set of linkages using the angle between time series in vector space (Murtagh and Contreras, 2012). We use the maximum distance (complete linkage) to split the linkage matrix, which is favorable because it ensures a minimum intra-cluster correlation. An average linkage scheme was tested and produced heterogeneous cluster sizes with outliers. We choose our cluster threshold from the hierarchical clustering dendrogram (~~Figure S2~~)Fig. S6), which maximizes cluster size while minimizing cluster internal diversity (~~Figure S3~~Fig. S7). We emphasize that the correlation is based on the temporal co-evolution of the time series, and is less sensitive to the relative magnitudes of peaks and troughs between data points. For an oscillating time series, the magnitude of the Pearson correlation coefficient is driven by the synchronization of peak timing, especially in normalized time series. The combination of several sensors in this study may impact

the magnitudes of the resultant time series, but will not have an outsized effect on the timing, and thus clustering, of our time series.

3 Results

3.1 Melt Algorithm Validation

3.1.1 Comparison with Manual Control Dataset

The agreement between manually clicked start/end dates and algorithm-derived start/end dates is generally within 3 days, with ~~more than~~ 70% or more of start and end dates falling within 5 days of the control dataset (Table 1). We find the lowest standard deviation for the end of melt, which is to be expected given that the end of snowmelt is determined by both snow clearance and the Tb_{37V} signal, and thus is more tightly constrained than the melt onset date. The melt onset date, while having a low average offset, has a high standard deviation as the algorithm sometimes has trouble correctly choosing the onset of melt when a snow season has several large storms, or several periods of melting and refreezing (cf. Fig. 3). Thus, errors in identification of melt onset will naturally have a higher standard deviation due to the presence of more relatively large misclassification errors.

Diverse snow seasons are shown from an example location (71.25E, 36.75N), over ~~four~~ six years of data (Fig. 3). Despite clear inter-annual variations in the temporal distribution of SWE, there exists high correlation between the algorithm-derived melt dates and our manually chosen melt dates. In the sample data, the first ~~shown snow season has~~ and third snow seasons have multiple peaks which could possibly be the true onset of the snowmelt season, and these years are flagged as unconstrained. The second and fourth years of data have a simple structure with a well-defined peak and a pseudo-linear melt during the spring season. The ~~second~~ fifth year of data has a ~~small melt pulse in the spring, followed by a large increase of SWE, causing a two-peaked SWE distribution. The third year has several small SWE peaks throughout the winter and spring, corresponding to phases of snowfall and brief periods of snowmelt. The final year~~ strong late-season XPGR peak, implying that the true start of the snowmelt season is not at the first peak. The last year of data shows a mismatch between the algorithm and control datasets, where it is difficult to determine the true onset of the snowmelt season. The algorithm picks the wider XPGR peak (earlier in the season), while we chose the thin but high peak later in the season as the start of snowmelt. Across all years of data shown ~~has a two-peaked SWE distribution, but the late-season storm does not deposit more snow than the early-season maximum. Despite drastic differences in SWE regimes between years,~~ here, the ~~main melt phase start and end dates were generally correctly identified~~ snowmelt end date is well matched between the algorithm and manual datasets.

3.1.2 Comparison with MODIS Snowcover Data

The MODIS sensor onboard Terra (product MOD10C1 V006, (K. and Riggs, 2016)) provides an additional estimate of snowcover from an optical, instead of PM, instrument. While MODIS cannot provide accurate measurements of fractional snow covered area (SCA) in the presence of clouds, it represents an independent control on the snowmelt end date (Fig. 4). In Figure 4A, the MODIS snow-clearance date is defined as the first day when five out of seven days have less than 5% SCA, and the data are

cloud free. Only those dates where there is no cloud cover within seven days of the end of the snowmelt season are used in Figure 4, which illustrates the consistently low SCA fraction at our algorithm-derived end of the snowmelt season.

3.1.3 Comparison with HAR Surface Temperature Data

HAR provides surface temperature at hourly intervals from 2000-2014 at 30 km spatial resolution over the entire study area (Maussion et al., 2014) . Using this data, we derive (1) the full-day average surface temperature, (2) the average daytime surface temperature, and (3) the daily surface temperature range at each melt onset date (Fig. ~~3~~5).

While the relationship between surface temperature and snowmelt onset isn't as clearly defined as the comparison between MODIS SCA and snowmelt end, the highly variable surface temperature and positive daytime surface temperature at the algorithm-derived snowmelt onset date implies that the algorithm correctly captures the increase in temperature variability at the onset of snowmelt.

3.2 Application: Spatial Patterns of Snowmelt Period

Using our melt tracking algorithm, we can identify the start and end dates of melt on a yearly basis. This also allows us to calculate the length of the snowmelt season, termed here the snowmelt period. The long-term average snowmelt period is shown in Figure 6.

The length of the snowmelt season varies significantly across HMA (Fig. 7). In many low-elevation areas, such as the Ganges Plain, and low-SWE areas, such as the central Tarim Basin, ~~snow is present for less than a month on average~~the snowmelt period is very short. Higher-elevation zones, and in particular the Tibetan Plateau, see ~~melt~~ snowmelt periods of several months. While both elevation and the amount of SWE impact snowmelt, these are not the sole determinants of snowmelt onset and end (Fig. 7). Each of the major catchments (cf. Fig. 1) has a unique melt start date, end date, and snowmelt-period distribution, based on the various climate and topographic forcings present in each catchment.

3.3 Hierarchical Clusters

Cluster selection criteria can be seen in Figures ~~S2-3~~S6-7. We base our selected dendrogram cutoff (distance threshold in vector space) on a combination of the number of generated clusters, the internal variation within those clusters, and the average resultant cluster size. In our case, we choose a distance cutoff of 1 radian from the complete linkage matrix (minimum intra-cluster correlation 0.525), which results in 285 clusters (Fig. 8).

While the hierarchical clusters are not based on any explicit spatial relationships, many of the clusters fall into spatially coherent groups. For example, the Pamir Knot and Tarim ~~basin~~ Basin both form large, coherent clusters based on the similarity of their snowfall and snowmelt patterns. The large number of small clusters throughout the Himalaya indicate that the region is not climatically uniform, and small-scale variations in topography and climate have strong impacts on the snowmelt regime.

4 Discussion

4.1 Spatial Melt Patterns from Hierarchical Clustering

As can be seen in Figure 3, inter-annual variation in ~~snowfall~~ the timing of snow buildup can cause large disparities in the yearly dates of snowmelt onset and end. This is particularly true of areas impacted by the WWD, which often have multiple snowfall events starting in winter and lasting until spring (Cannon et al., 2014). This complicates change detection of the onset of melt between years, as one year may receive a small late season storm, and thus start the major snowmelt phase in the spring, while the next year may receive a large summer storm, and thus start its main snowmelt phase in the summer.

To mitigate the influence of inter-annual variation in determining long-term trends in snowmelt onset and end, we group our data into self-similar clusters using hierarchical clustering. We do not filter our generated clusters based on size or self-similarity, as we do not use our clusters to generate a single averaged or representative time series for each cluster, as is often done in climate analyses. Due to inter-annual variations in SWE, and snowmelt onset/end dates, fitting a linear regression through only 29 years of data does not provide statistically significant results for the majority of HMA. Instead, we use our clusters to group sets of algorithmically-derived melt onset and end dates, and fit linear models on a cluster-by-cluster basis. By leveraging the melt start and end dates of a set of time series in parallel, we are able to identify statistically significant changes in melt onset and end dates, as well as changes in the length of the snowmelt period (Fig. 9). To reduce noise from low-SWE and very short snowmelt period areas, we remove areas from the subsequent analyses with long-term average melt periods of less than 20 days. We also remove melt onset dates that are flagged as unconstrained (when there are multiple candidate snowmelt onset dates) to limit the impact of unreliable melt onset data on our analysis.

~~Changes in snowmelt onset date are split between earlier melt onset (negative trend) outside of the Tibetan Plateau, and slightly later onset (positive~~ Snowmelt onset is trending earlier (negative trend) in ~~many high elevation areas~~ HMA outside of a small band running from the Karakoram through the interior Tibetan Plateau (Fig. 9A). Negative snowmelt onset trends have been previously observed in Central Asia (Lioubimtseva and Henebry, 2009; Dietz et al., 2014)~~and~~ , the Himalaya (Lau et al., 2010; Panday et al., 2011), and the Tibetan Plateau (Xu et al., 2017) , but have not been confirmed a with decadal-timescale, large-area and empirical study of snowmelt dates.

~~Increasing~~ A complex pattern of regionally increasing and decreasing spring snow depth ~~has been observed across~~ in the Tibetan Plateau has been observed since the 1970s ~~(Zhang et al., 2004; Che et al., 2008)~~ (Zhang et al., 2004; Che et al., 2008; Wang et al., 20 which could help account for the ~~later onset~~ mixed onset trends observed in the ~~majority of the~~ Tibetan Interior. High-elevation zones in the upper Indus catchment, running from the Karakorum in a south-eastward direction, have seen increased precipitation over the past decades due to increases in the strength of the WWD (Cannon et al., 2015; Norris et al., 2016; Treydte et al., 2006). ~~Changes in the eastern Himalaya are likely driven by a combination of late season storms, increased snowfall over the past decades, and the very high average elevation of this region (Stewart, 2009) .~~

Temperatures in HMA are increasing faster than the global average (Vaughan et al., 2013; Lau et al., 2010), and are likely the primary driver of the almost universal earlier snowmelt end dates as seen in Figure 9B. Increased temperatures have likely both

reduced overall SWE amounts, by causing more precipitation to fall as rain, and decreased SWE persistence into the spring and summer months. These changes have helped drive a 2-8 day/decade earlier end to the snowmelt season (Fig. 9B).

The length of the snowmelt season is shortening in much of HMA, with the exception of ~~an area running from the Pamirto Kunlun Shan~~small areas in the Pamir, Tien Shan, and Karakoram regions (Fig. 9C). We attribute this to a combination of increased storm intensity in the WWD, and increases in late season storms, which could help extend the snowmelt season slightly later into the year (Cannon et al., 2016; Norris et al., 2015; Kapnick et al., 2014). In general, however, the snowmelt season is shortening throughout HMA. Intensification of the spring runoff regime in HMA has been observed in both model (Lutz et al., 2014) and empirical (Dietz et al., 2014; Bookhagen and Burbank, 2010; Stewart, 2009) data.

4.2 Temporal Heterogeneity in Snowmelt Trends

Not only are changes in the snowmelt regime spatially complex (e.g., Fig. 9), but they exhibit distinct temporal heterogeneity as well.

Changes in snowmelt onset do not have a bias towards early or late onset snow regimes (Fig. 10A). The end of the snowmelt season is almost universally negative (earlier), excepting a few ~~early-onset zones. These zones are predominantly low-SWE, short melt-season, areas~~ isolated areas in the Kunlun Shan (cf. Fig. 9). The majority of locations show negative (shorter) trends in snowmelt period. Strong negative changes in the snowmelt period are biased towards areas with long melt seasons (120 days or more). This implies that high-elevation areas, such as the Tibetan Plateau, and high-SWE areas, such as the Karakoram, will see a relatively stronger compression in the length of the snowmelt season. While changes in the snowmelt onset date are partially responsible, the main driver of shorter snowmelt periods is the earlier end of the snowmelt season across most of HMA.

Several-decade long trends conceal short-term fluctuations in the snowmelt regime of HMA. To assess the impact of the analysis timeframe on our regression results, we analyzed trends with window sizes ranging from four years to 28 years, across all possible start-year and window-size combinations, averaged over the entire study area (Fig. 11).

Trends are universally negative for the onset and end of the snowmelt season, as well as for the snowmelt period, between 1988 and 1995, regardless of the timeframe over which the regression is performed. While there were some short positive trends in snowmelt end date (5-10 years) starting in the mid 1990s, trends in end dates and snowmelt period are generally negative. Although long-term trends in snowmelt onset date (longer than 20 years) are negative, recent trends (after 2002) in snowmelt onset date are positive when considered at timeframes of 5-10 years. This implies that while the three-decade trend in snowmelt onset dates has been negative, the trend has become more variable in the past decade.

It is clear that decadal trends (cf. Fig. 9) are not consistent throughout the entire study period (cf. Fig. 11). When trends in the first half (1988-2002) and second half (2002-2016) of the data are compared, distinct regional patterns are apparent (Fig. 12).

The lack of statistically significant trends limits some interpretations, particularly with regards to changes in the snowmelt period. ~~Only small parts of the Tibetan Plateau and the eastern Himalaya have maintained trends towards later snowmelt onset through~~ Nowhere in HMA are snowmelt onset trends consistent in both analysis periods. While many snowmelt end dates have

remained negative in both time periods, trends in parts of the Pamir and Karakoram have moved from negative to positive, and those in the Tien Shan have become less negative (cf~~Fig. S4~~. Fig. S8). A similar story is apparent when snowmelt onset dates are considered, where the Tien Shan and parts of the Pamir have moved from negative to positive snowmelt onset dates. Unfortunately, due the the climatically short nature of the dataset, it is not clear whether this change represents inter-annual variability or a reversal of a long-term trend.

4.3 Hydrologic Implications

The spatially and topographically complex changes in snowmelt onset, end, and period make interpretation of downstream impacts difficult. The long-term trend in HMA of a shortened and earlier melt season will impact downstream populations who rely on the consistent timing and volume of spring and summer runoff (Archer and Fowler, 2004; Barnett et al., 2005). Already the impacts of precipitation intensification and shifts in the snowmelt season have been felt in many regions (Barnett et al., 2005; Stewart, 2009). These trends are likely to continue as temperatures rise across HMA, and each major catchment will feel the impacts of a shortened snowmelt season, regardless of changes in the start and end dates of melt.

Many regions rely on glaciers as their only water source between the end of snowmelt and the beginning of major precipitation systems (Bolch et al., 2012). This important water reserve is certain to be impacted by, and reflect changes in, the snowmelt regime of HMA, as the timing of precipitation has been shown to be an important factor in the response of glaciers to climate change ~~(?Wang et al., 2017)~~ (Maussion et al., 2014; Wang et al., 2017) . While many regions have seen rapid glacier retreat (Bolch et al., 2012; Kääb et al., 2012, 2015; Scherler et al., 2011) there exist regions of glacier stability and even growth, such as the Karakoram (Hewitt, 2005; Gardelle et al., 2012) and Kunlun Shan (Gardner et al., 2013; Yao et al., 2012). Our results (cf. Fig. 9) show longer snowmelt periods in parts of the Pamir~~and Kunlun Shan~~, later snowmelt ~~onset~~ end dates in parts of the Karakoram and Kunlun Shan, and relatively less negative trends in snowmelt end in the Pamir ~~, Karakoram, and Kunlun Shan~~ when compared with the rest of HMA. These regions overlap with both the 'Karakoram Anomaly' and positive glacier mass balances in parts of the Kunlun Shan and Pamir, implying that changes in the timing of the snowmelt season could be partially responsible for regional heterogeneity in glacier change.

The majority of HMA, however, exhibits a three-decade long trend towards an earlier end of the snowmelt season. Earlier snow clearance increases the absorption of solar radiation, and thus stores more heat at high elevations and generates a positive feedback (Willis et al., 2002). As seasonal snow is removed earlier from glacier regions, glacier melt will accelerate. In general, glaciers in HMA are decreasing in volume and shrinking, which fits with the observed long-term decrease in snowmelt end dates (cf. Figs. 9, 10, 11), despite clear spatial and temporal heterogeneity in these trends (cf. Fig. 12).

4.4 Caveats of the Method

Our algorithm-derived snowmelt end dates and the snowmelt end dates derived from the independent MOD10C1 product show close alignment, indicating that the algorithm is well-suited to identifying the end of the snowmelt season (cf. Fig. 4). The identification of the onset of the snowmelt season, however, is more difficult. Periods of melt and refreeze, as well as

late-season storms, hamper the identification of a single snowmelt onset date. Furthermore, without rigorous measurements of surface air temperature or in-situ monitoring of snowmelt, the efficacy of our algorithm cannot be directly confirmed.

Snowmelt onset dates are correlated with the day of year that HAR temperatures first start to increase (Fig. S2). Furthermore, they are associated with days with a high temperature range and on-average positive daytime surface temperatures (cf. Fig. 5). This implies that rising daytime temperatures, in conjunction with solar radiation, induce the start of the snowmelt season in our study area. However, as we lack a direct control dataset for snowmelt onset, and there is a high degree of variance in the HAR surface temperature-snowmelt onset relationship, snowmelt onset dates and trends therein should be considered as less reliable than snowmelt end dates.

5 Conclusions

This study presents a snowmelt tracking algorithm based on the cross-polarized gradient ratio, native passive microwave (PM) signal, and a rough estimate of snow-water equivalent (SWE). We do not rely on static thresholds to determine the onset or end of the snowmelt season across our diverse study region, but instead rely on identifying the snowmelt signal from intrinsic properties of each individual time series. The algorithm leverages passive microwave data from the Special Sensor Microwave/Imager (SSMI), Special Sensor Microwave Imager/Sounder (SSMIS), Advanced Microwave Scanning Radiometer - Earth Observing System (AMSR-E), AMSR2, and Global Precipitation Measurement (GPM) satellites (1987-2016) to track the onset, duration, and end of the snowmelt season across High Mountain Asia (HMA). We examine large-scale spatial patterns in the snowmelt regime and identify trends in the timing of snowmelt across HMA over the past three decades using hierarchical clustering.

We find the following four key points: (1) The snowmelt season is ending earlier in much of HMA (negative trend), with magnitudes between 2 and 8 days/decade (5-25 days total over 29 years). The length of the snowmelt season is shortening in the majority of HMA, despite some regions of delayed snowmelt onset. (2) Negative changes to the end of the snowmelt season are felt most strongly in areas with long snowmelt seasons (as averaged over three decades), such as the Tibetan Plateau and high-SWE areas in the Himalaya, Karakoram, and Tien Shan. (3) While three-decade long trends indicate earlier start and end dates for the snowmelt season, recent (2002-2016) trends are positive (later snowmelt end dates) in many regions of HMA. These changes could be due to inter-annual variability or a reversal in the long-term trend. (4) Areas with slightly longer snowmelt seasons or later onset dates overlap with regions of positive glacier mass balance, such as the ~~Karakoram~~ Pamir and Kunlun Shan. This implies that changes to the snowmelt regime of HMA could help account for some of the observed regional glacier changes. In general, however, regional warming has caused long-term earlier snowmelt onset and shortened melt seasons in much of HMA. These changes are spatially and temporally complex, and will require further local and high-spatial resolution assessments to fully understand changes in HMA's cryosphere.

Code availability. The code used in this study is available online at: https://github.com/UP-RS-ESP/SnowmeltTracking

Author contributions. T.S. and B.B. designed the study, T.S. prepared and analyzed the PM data. B.B. and A.R. contributed to the development of the methodology. T.S. wrote the manuscript with input from all authors.

Competing interests. The authors declare that they have no conflict of interest.

References

Abdalati, W. and Steffen, K.: Passive microwave-derived snow melt regions on the Greenland Ice Sheet, Geophysical Research Letters, 22, 787–790, 1995.

Apgar, J. D., Ramage, J. M., McKenney, R. A., and Maltais, P.: AMSR-E algorithm for snowmelt onset detection in sub-arctic heterogeneous terrain, Hydrological processes, 21, 1587–1596, 2007.

Archer, D. R. and Fowler, H.: Spatial and temporal variations in precipitation in the Upper Indus Basin, global teleconnections and hydrological implications, Hydrology and Earth System Sciences Discussions, 8, 47–61, 2004.

Armstrong, R. and Brodzik, M.: Recent Northern Hemisphere snow extent: A comparison of data derived from visible and microwave satellite sensors, Geophysical Research Letters, 28, 3673–3676, 2001.

Barnett, T. P., Adam, J. C., and Lettenmaier, D. P.: Potential impacts of a warming climate on water availability in snow-dominated regions, Nature, 438, 303–309, 2005.

Bolch, T., Kulkarni, A., Kääb, A., Huggel, C., Paul, F., Cogley, J., Frey, H., Kargel, J., Fujita, K., Scheel, M., et al.: The state and fate of Himalayan glaciers, Science, 336, 310–314, 2012.

Bookhagen, B.: Chapter 11: The influence of Hydrology and Glaciology on Wetlands in the Himalaya, in: Bird Migration Across the Himalayas: Wetland Functioning Amidst Mountains and Glaciers, edited by Prins, H. and Namgail, T., Cambridge University press, 2017.

Bookhagen, B. and Burbank, D. W.: Toward a complete Himalayan hydrological budget: Spatiotemporal distribution of snowmelt and rainfall and their impact on river discharge, Journal of Geophysical Research: Earth Surface (2003–2012), 115, 2010.

Cannon, F., Carvalho, L., Jones, C., and Bookhagen, B.: Multi-annual variations in winter westerly disturbance activity affecting the Himalaya, Climate Dynamics, pp. 1–15, 2014.

Cannon, F., Carvalho, L. M., Jones, C., and Norris, J.: Winter westerly disturbance dynamics and precipitation in the western Himalaya and Karakoram: a wave-tracking approach, Theoretical and Applied Climatology, pp. 1–18, 2015.

Cannon, F., Carvalho, L., Jones, C., Hoell, A., Norris, J., Kiladis, G., and Tahir, A.: The influence of tropical forcing on extreme winter precipitation in the western Himalaya, Climate Dynamics, 2016.

Cannon, F., Carvalho, L. M. V., Jones, C., Norris, J., Bookhagen, B., and Kiladis, G. N.: Effects of Topographic Smoothing on the Simulation of Winter Precipitation in High Mountain Asia, Journal of Geophysical Research: Atmospheres, pp. n/a–n/a, doi:10.1002/2016JD026038, http://dx.doi.org/10.1002/2016JD026038, 2016JD026038, 2017.

Chang, A., Foster, J., and Hall, D.: Nimbus-7 SMMR derived global snow cover parameters, Annals of glaciology, 9, 39–44, 1987.

Che, T., Xin, L., Jin, R., Armstrong, R., and Zhang, T.: Snow depth derived from passive microwave remote-sensing data in China, Annals of Glaciology, 49, 145–154, 2008.

Corpet, F.: Multiple sequence alignment with hierarchical clustering, Nucleic acids research, 16, 10 881–10 890, 1988.

Dahe, Q., Shiyin, L., and Peiji, L.: Snow cover distribution, variability, and response to climate change in western China, Journal of climate, 19, 1820–1833, 2006.

Daly, S. F., Vuyovich, C. M., Deeb, E. J., Newman, S. D., Baldwin, T. B., and Gagnon, J. J.: Assessment of the snow conditions in the major watersheds of Afghanistan using multispectral and passive microwave remote sensing, Hydrological Processes, 26, 2631–2642, 2012.

Dietz, A. J., Conrad, C., Kuenzer, C., Gesell, G., and Dech, S.: Identifying changing snow cover characteristics in Central Asia between 1986 and 2014 from remote sensing data, Remote Sensing, 6, 12 752–12 775, 2014.

Drobot, S. D. and Anderson, M. R.: An improved method for determining snowmelt onset dates over Arctic sea ice using scanning multichannel microwave radiometer and Special Sensor Microwave/Imager data, 2001.

Gardelle, J., Berthier, E., and Arnaud, Y.: Slight mass gain of Karakoram glaciers in the early twenty-first century, Nature geoscience, 5, 322–325, 2012.

Gardner, A. S., Moholdt, G., Cogley, J. G., Wouters, B., Arendt, A. A., Wahr, J., Berthier, E., Hock, R., Pfeffer, W. T., Kaser, G., et al.: A reconciled estimate of glacier contributions to sea level rise: 2003 to 2009, Science, 340, 852–857, 2013.

Hall, D. K., Williams Jr, R. S., Steffen, K., and Chien, J. Y.: Analysis of summer 2002 melt extent on the Greenland Ice Sheet using MODIS and SSM/I data, in: Geoscience and Remote Sensing Symposium, 2004. IGARSS'04. Proceedings. 2004 IEEE International, vol. 5, pp. 3029–3032, IEEE, 2004.

Hewitt, K.: The Karakoram anomaly? Glacier expansion and the'elevation effect,'Karakoram Himalaya, Mountain Research and Development, 25, 332–340, 2005.

Immerzeel, W. and Bierkens, M.: Asia's water balance, Nature Geoscience, 5, 841–842, 2012.

Immerzeel, W. W., Van Beek, L. P., and Bierkens, M. F.: Climate change will affect the Asian water towers, Science, 328, 1382–1385, 2010.

Jain, A. K., Murty, M. N., and Flynn, P. J.: Data clustering: a review, ACM computing surveys (CSUR), 31, 264–323, 1999.

Johnson, S. C.: Hierarchical clustering schemes, Psychometrika, 32, 241–254, 1967.

Joshi, M., Merry, C. J., Jezek, K. C., and Bolzan, J. F.: An edge detection technique to estimate melt duration, season and melt extent on the Greenland ice sheet using passive microwave data, Geophysical Research Letters, 28, 3497–3500, 2001.

K., D. and Riggs, G. A.: MODIS/Terra Snow Cover Daily L3 Global 0.05Deg CMG, Version 6, http://dx.doi.org/10.5067/MODIS/MOD10C1.006.27.6.2017, 2016.

Kääb, A., Berthier, E., Nuth, C., Gardelle, J., and Arnaud, Y.: Contrasting patterns of early twenty-first-century glacier mass change in the Himalayas, Nature, 488, 495–498, 2012.

Kääb, A., Treichler, D., Nuth, C., and Berthier, E.: Brief Communication: Contending estimates of 2003–2008 glacier mass balance over the Pamir–Karakoram–Himalaya, The Cryosphere, 9, 557–564, 2015.

Kang, S., Xu, Y., You, Q., Flügel, W.-A., Pepin, N., and Yao, T.: Review of climate and cryospheric change in the Tibetan Plateau, Environmental Research Letters, 5, 015 101, 2010.

Kapnick, S. B., Delworth, T. L., Ashfaq, M., Malyshev, S., and Milly, P.: Snowfall less sensitive to warming in Karakoram than in Himalayas due to a unique seasonal cycle, Nature Geoscience, 7, 834–840, 2014.

Kelly, R.: The AMSR-E snow depth algorithm: Description and initial results, 29, 307–317, 2009.

Kelly, R. E., Chang, A. T., Tsang, L., and Foster, J. L.: A prototype AMSR-E global snow area and snow depth algorithm, Geoscience and Remote Sensing, IEEE Transactions on, 41, 230–242, 2003.

Lau, W. K., Kim, M.-K., Kim, K.-M., and Lee, W.-S.: Enhanced surface warming and accelerated snow melt in the Himalayas and Tibetan Plateau induced by absorbing aerosols, Environmental Research Letters, 5, 025 204, 2010.

Lioubimtseva, E. and Henebry, G. M.: Climate and environmental change in arid Central Asia: Impacts, vulnerability, and adaptations, Journal of Arid Environments, 73, 963–977, 2009.

Liu, H., Wang, L., and Jezek, K. C.: Wavelet-transform based edge detection approach to derivation of snowmelt onset, end and duration from satellite passive microwave measurements, International Journal of Remote Sensing, 26, 4639–4660, 2005.

Lutz, A., Immerzeel, W., Shrestha, A., and Bierkens, M.: Consistent increase in High Asia's runoff due to increasing glacier melt and precipitation, Nature Climate Change, 4, 587–592, 2014.

Malik, N., Bookhagen, B., and Mucha, P. J.: Spatiotemporal patterns and trends of Indian monsoonal rainfall extremes, Geophysical Research Letters, 43, 1710–1717, 2016.

Maussion, F., Scherer, D., Mölg, T., Collier, E., Curio, J., and Finkelnburg, R.: Precipitation Seasonality and Variability over the Tibetan Plateau as Resolved by the High Asia Reanalysis*, Journal of Climate, 27, 1910–1927, 2014.

Monahan, P. A. and Ramage, J.: AMSR-E melt patterns on the Southern Patagonia Icefield, Journal of Glaciology, 56, 699–708, 2010.

Murtagh, F. and Contreras, P.: Algorithms for hierarchical clustering: an overview, Wiley Interdisciplinary Reviews: Data Mining and Knowledge Discovery, 2, 86–97, 2012.

Norris, J., Carvalho, L. M., Jones, C., and Cannon, F.: WRF simulations of two extreme snowfall events associated with contrasting extratropical cyclones over the western and central Himalaya, Journal of Geophysical Research: Atmospheres, 120, 3114–3138, 2015.

Norris, J., Carvalho, L. M., Jones, C., Cannon, F., Bookhagen, B., Palazzi, E., and Tahir, A. A.: The spatiotemporal variability of precipitation over the Himalaya: evaluation of one-year WRF model simulation, Climate Dynamics, pp. 1–26, 2016.

Panday, P. K., Frey, K. E., and Ghimire, B.: Detection of the timing and duration of snowmelt in the Hindu Kush-Himalaya using QuikSCAT, 2000–2008, Environmental Research Letters, 6, 024 007, 2011.

Rheinwalt, A.: Python C-extension for memory efficient and multithreaded Pearson product-moment correlation coefficient estimation using OpenMP, https://github.com/UP-RS-ESP/CorrCoef, 2016.

Rheinwalt, A.: Normalize time series by quantile normalization to the normal distribution., https://github.com/UP-RS-ESP/CorrCoef, https://github.com/UP-RS-ESP/Normalize, 2017.

Rheinwalt, A., Goswami, B., Boers, N., Heitzig, J., Marwan, N., Krishnan, R., and Kurths, J.: Teleconnections in Climate Networks: A Network-of-Networks Approach to Investigate the Influence of Sea Surface Temperature Variability on Monsoon Systems, in: Machine Learning and Data Mining Approaches to Climate Science, pp. 23–33, Springer, 2015.

Scherler, D., Bookhagen, B., and Strecker, M. R.: Spatially variable response of Himalayan glaciers to climate change affected by debris cover, Nature Geoscience, 4, 156–159, 2011.

Shrestha, M., Koike, T., Hirabayashi, Y., Xue, Y., Wang, L., Rasul, G., and Ahmad, B.: Integrated simulation of snow and glacier melt in water and energy balance-based, distributed hydrological modeling framework at Hunza River Basin of Pakistan Karakoram region, Journal of Geophysical Research: Atmospheres, 120, 4889–4919, 2015.

Smith, T. and Bookhagen, B.: Assessing uncertainty and sensor biases in passive microwave data across High Mountain Asia, Remote Sensing of Environment, 181, 174–185, 2016.

Stewart, I. T.: Changes in snowpack and snowmelt runoff for key mountain regions, Hydrological Processes, 23, 78–94, 2009.

Takala, M., Pulliainen, J., Huttunen, M., and Hallikainen, M.: Estimation of the beginning of snow melt period using SSM/I data, in: Geoscience and Remote Sensing Symposium, 2003. IGARSS'03. Proceedings. 2003 IEEE International, vol. 4, pp. 2841–2843, IEEE, 2003.

Takala, M., Pulliainen, J., Huttunen, M., and Hallikainen, M.: Detecting the onset of snow-melt using SSM/I data and the self-organizing map, International Journal of Remote Sensing, 29, 755–766, 2008.

Takala, M., Pulliainen, J., Metsämäki, S. J., and Koskinen, J. T.: Detection of snowmelt using spaceborne microwave radiometer data in Eurasia from 1979 to 2007, Geoscience and Remote Sensing, IEEE Transactions on, 47, 2996–3007, 2009.

Takala, M., Luojus, K., Pulliainen, J., Derksen, C., Lemmetyinen, J., Kärnä, J.-P., Koskinen, J., and Bojkov, B.: Estimating northern hemisphere snow water equivalent for climate research through assimilation of space-borne radiometer data and ground-based measurements, Remote Sensing of Environment, 115, 3517–3529, 2011.

Tedesco, M.: Snowmelt detection over the Greenland ice sheet from SSM/I brightness temperature daily variations, Geophysical Research Letters, 34, 2007.

Tedesco, M. and Narvekar, P. S.: Assessment of the NASA AMSR-E SWE Product, Selected Topics in Applied Earth Observations and Remote Sensing, IEEE Journal of, 3, 141–159, 2010.

Tedesco, M., Derksen, C., Deems, J. S., and Foster, J. L.: Remote sensing of snow depth and snow water equivalent, Remote Sensing of the Cryosphere, pp. 73–98, 2015.

Treydte, K. S., Schleser, G. H., Helle, G., Frank, D. C., Winiger, M., Haug, G. H., and Esper, J.: The twentieth century was the wettest period in northern Pakistan over the past millennium, Nature, 440, 1179–1182, 2006.

Vaughan, D., Comiso, J., Allison, I., Carrasco, J., Kaser, G., Kwok, R., Mote, P., Murray, T., Paul, F., Ren, J., Rignot, E., Solomina, O., Steffen, K., and Zhang, T.: Observations: Cryosphere. In: Climate Change 2013: The Physical Science Basis., Contribution of Working Group I to the Fifth Assessment Report of the IPCC., 2013.

Wang, Q., Yi, S., and Sun, W.: Precipitation-driven glacier changes in the Pamir and Hindu Kush mountains, Geophysical Research Letters, pp. n/a–n/a, doi:10.1002/2017GL072646, http://dx.doi.org/10.1002/2017GL072646, 2017.

Wang, T., Peng, S., Lin, X., and Chang, J.: Declining snow cover may affect spring phenological trend on the Tibetan Plateau, Proceedings of the National Academy of Sciences, 110, E2854–E2855, 2013.

Wentz, F. J.: SSM/I version-7 calibration report, Remote Sensing Systems Rep, 11012, 46, 2013.

Willis, I. C., Arnold, N. S., and Brock, B. W.: Effect of snowpack removal on energy balance, melt and runoff in a small supraglacial catchment, Hydrological Processes, 16, 2721–2749, doi:10.1002/hyp.1067, http://dx.doi.org/10.1002/hyp.1067, 2002.

Xu, W., Ma, L., Ma, M., Zhang, H., and Yuan, W.: Spatial–temporal variability of snow cover and depth in the Qinghai–Tibetan Plateau, Journal of Climate, 30, 1521–1533, 2017.

Yao, T., Thompson, L., Yang, W., Yu, W., Gao, Y., Guo, X., Yang, X., Duan, K., Zhao, H., Xu, B., et al.: Different glacier status with atmospheric circulations in Tibetan Plateau and surroundings, Nature Climate Change, 2, 663–667, 2012.

Zhang, Y., Li, T., and Wang, B.: Decadal change of the spring snow depth over the Tibetan Plateau: the associated circulation and influence on the east Asian summer monsoon*, Journal of Climate, 17, 2780–2793, 2004.

Table 1. Summary statistics comparing ~~the~~ manual control dataset and ~~the~~ algorithm dataset (n=2100, 28 snowmelt seasons at 25 locations).

Variable	Mean Offset (days)	Mean Absolute Offset (days)	Standard Deviation	RMSE	Percentage of Algorithm Dates Within 3/5/10 Days of Control Dates
Snowmelt Onset	~~0.98~~ -0.23	~~6.82~~ 5.51	~~19.22~~ 16.71	~~19.25~~ 16.71	~~71~~ 68 / ~~77~~ 80 / ~~87~~ 90 %
Snowmelt End	~~-0.70~~ -1.3	~~4.70~~ 5.0	~~9.82~~ 9.74	~~9.84~~ 9.82	~~57~~ 49 / ~~74~~ 70 / ~~87~~ 89 %
Snowmelt Period	~~-1.61~~ -0.25	~~9.98~~ 7.44	~~21.08~~ 16.1	~~21.14~~ 16.1	~~46~~ 47 / ~~61~~ 64 / ~~75~~ 82 %

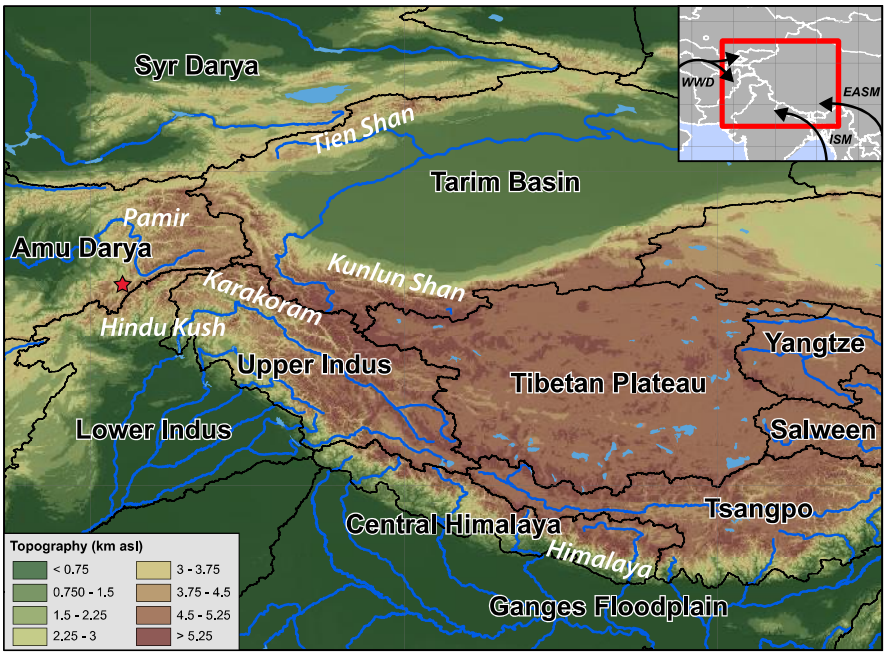

Figure 1. Topographic map of the study area across High Mountain Asia (HMA), with major catchment boundaries (black lines and labels in black font with white border) and major mountain ranges (white font). Inset map shows wind direction of major Asian weather systems (WWD: Winter Westerly Disturbances, ISM: Indian Summer Monsoon, EASM: East Asian Summer Monsoon) on top of political boundaries. Red star indicates the location used for Figures 2 and 3.

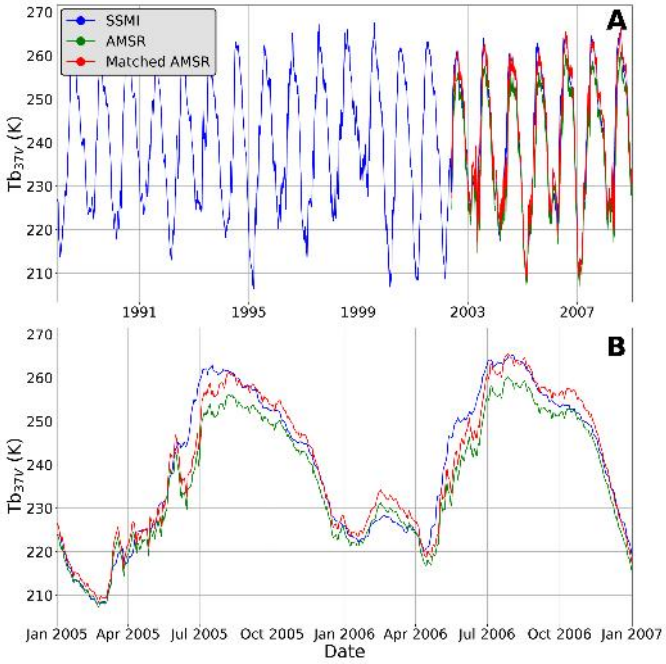

Figure 2. (~~a~~A) Sample time series showing SSMI (blue) and AMSR-E (green) Tb_{37V} frequencies, with linearly matched modified AMSR-E Tb (red), 1987-2009. Data taken from 71.25E, 36.75N (cf. Fig. 1). (~~b~~B) The same data as panel A but for two seasons (2005-2007).

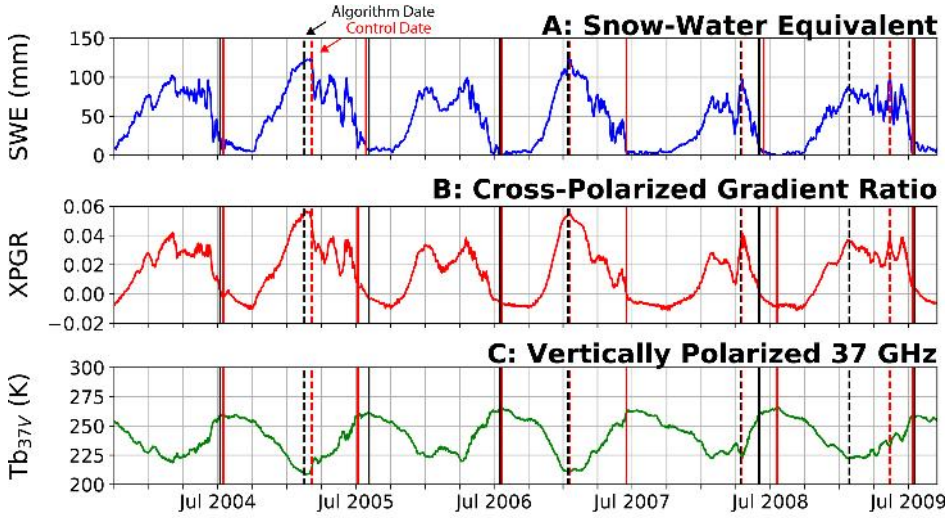

Figure 3. Sample data from 71.25E, 36.75N (cf. Fig. 1) showing: (~~a~~A) Snow-Water Equivalent (SWE) based on the Chang algorithm (Chang et al., 1987), (~~b~~B) Cross-Polarized Gradient Ratio (XPGR), and (~~c~~C) vertically polarized temperature brightness at 37 GHz (Tb_{37V}) measurements. Onset of melt (dashed lines) and end of melt (solid lines) are black for algorithm dates, and red for control dates. Lack of red lines indicates temporal overlap of algorithm and control dates. Years with multiple distinct peaks (e.g., 2004, 2006) are flagged as unconstrained, and not used for further analysis. We use the XPGR to identify the start of melt, and the SWE and Tb_{37V} measurements to identify the end of the melt season.

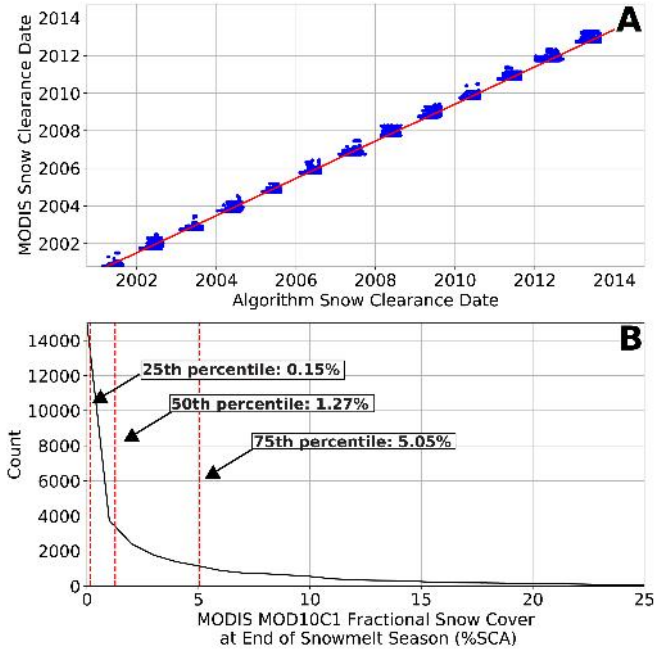

Figure 4. (A) Comparison of MODIS MOD10C1 (K. and Riggs, 2016) and algorithm-derived end of the snowmelt season dates and (B) MODIS snow covered area fraction at the algorithm-derived end of the snowmelt season. We find high agreement between the melt end dates derived from both datasets (slope = 1.00, R^2=0.99, n=34,468), and that the MODIS SCA is below 5% in the majority of derived end dates.

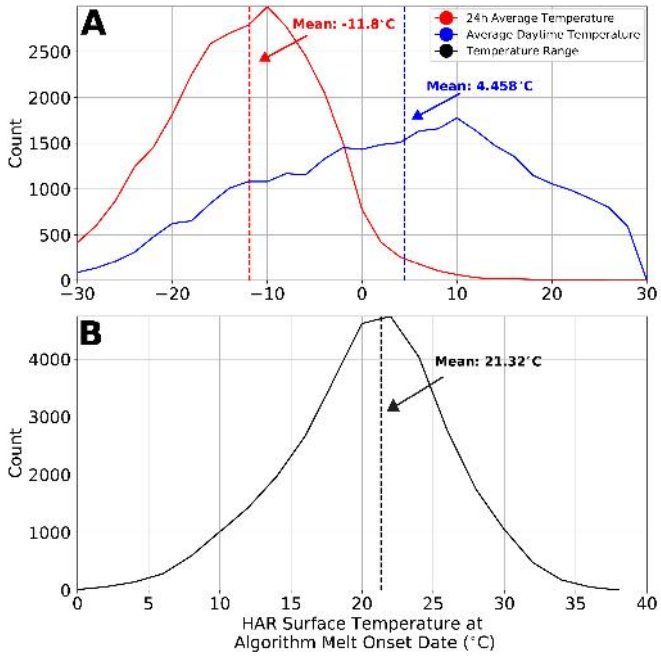

Figure 5. (A) HAR full-day average surface temperature (red), daytime average surface temperature (blue), and (B) daily surface temperature range (black) at the algorithm-derived snowmelt onset date (n=31,583). Full-day and daytime average temperatures show distinctly different distributions, with full-day temperatures averaging below 0°C and daytime temperatures above. This relationship, as well as the large daily temperature range, imply that the algorithm-derived melt onset dates occur at or near the transition from sub-freezing to above-freezing temperatures.

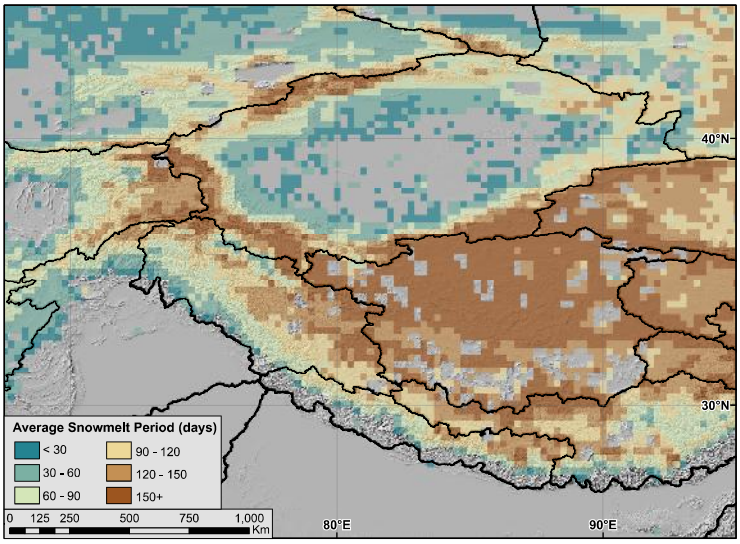

Figure 6. Average snowmelt period across HMA from 1987-2016. Snowmelt period ranges from less than a month to several months, depending on geographic location, elevation, and local climate. Locations with long-term average snowmelt periods less than 20 days are removed. Topographic hillshade in background. Grey areas indicate water bodies, low-SWE areas, and very short snowmelt period areas that are all excluded from the analysis.

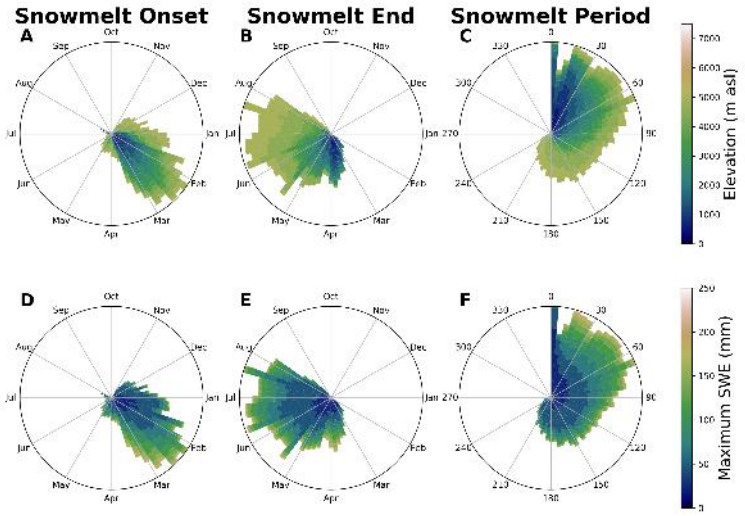

Figure 7. Snowmelt onset (A,D), end (B,E), and period (C,F) for the entire study area, colored by elevation (A-C) and snow depth (D-F) bins. Bin heights indicate relative number of pixels at each day of year (i.e. area). While very short snowmelt periods show a distinct low-elevation, low-SWE bias, in general melt onset and end dates are well distributed throughout elevation zones and SWE amounts.

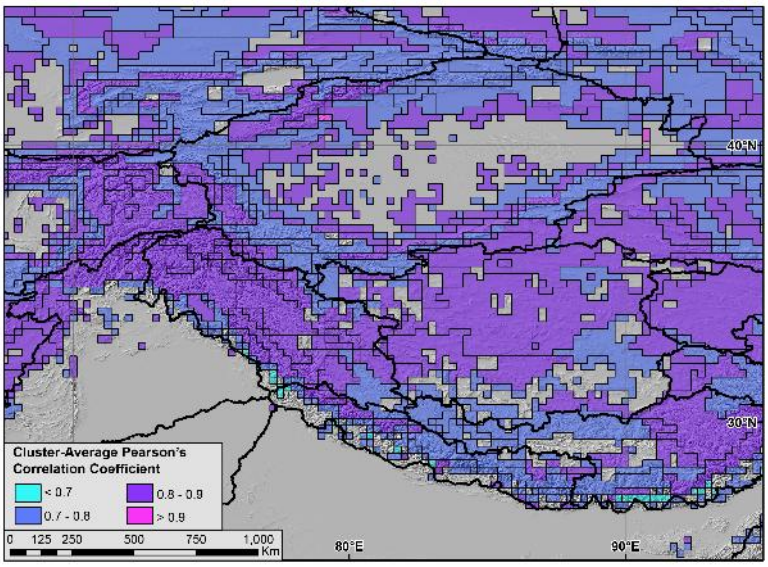

Figure 8. Hierarchical clusters (black outlines), as determined from the rank-order correlation coefficients of the 5-day resampled, merged, and linearly matched XPGR data (1987-2016). Colors indicate cluster-average internal diversity (average Pearson's correlation coefficient between members in the same cluster). Grey areas indicate water bodies, low-SWE areas excluded from the analysis, or areas with irregular PM signals which fail to cluster.

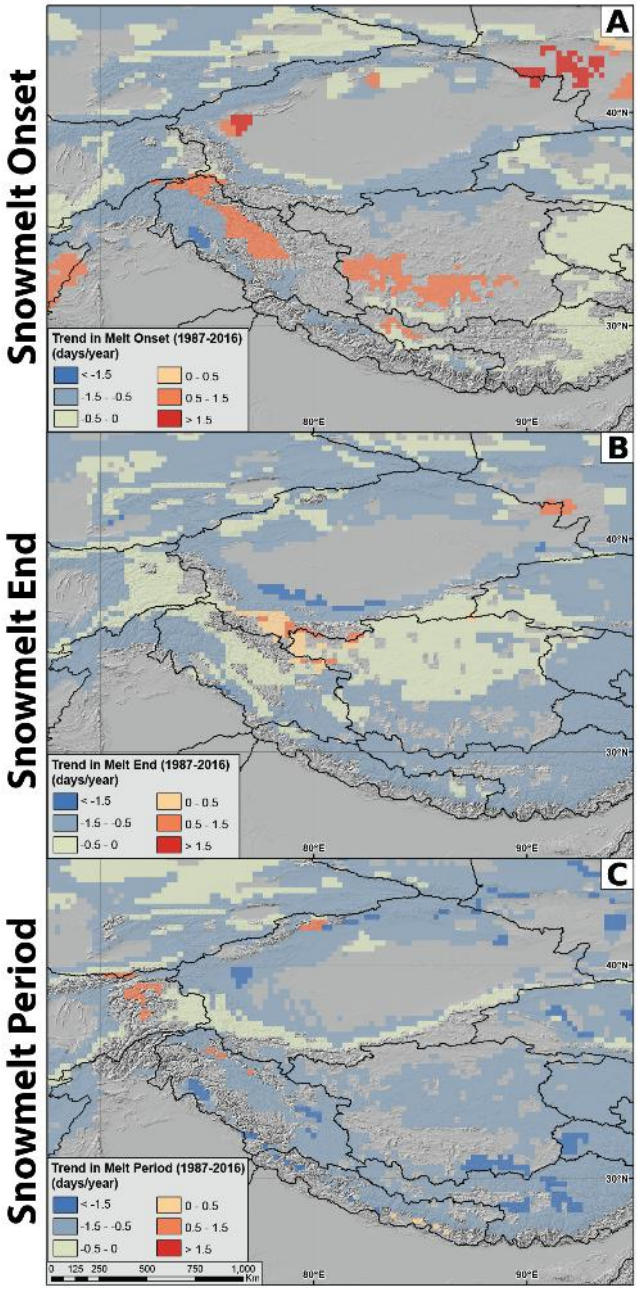

Figure 9. Significant (p <0.05) trends in date of snowmelt (~~a~~A) onset, (~~b~~B) end, and (~~c~~C) period, 1987-2016 for the cluster areas (cf. Fig. 8). The onset of snowmelt is generally moving earlier outside of the Tibetan ~~Plateau~~Plateau-Karakoram region, and moving slightly later in a high-elevation zone running from the Karakoram through the Tibetan Plateau interior, as well as parts of the Himalaya. The end of the melt season is moving earlier in the vast majority of HMA, at varying rates. Consequently, snowmelt period is also shrinking in much of HMA, with the exception of ~~parts of the Kunlun Shan along the northern edge of the Tibetan Plateau and~~ small parts of the Pamir, Karakoram, and Tien Shan.

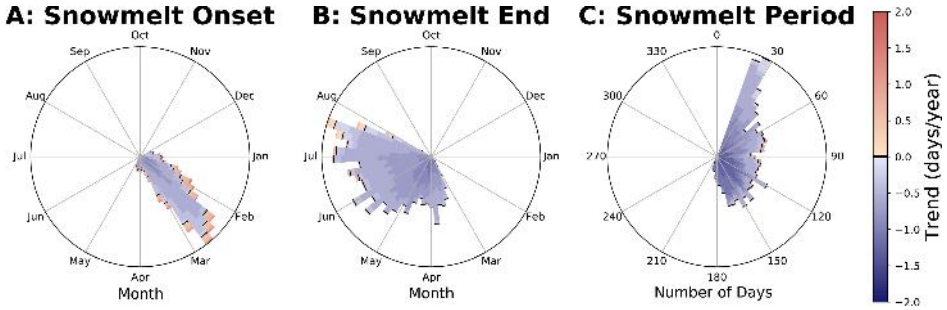

Figure 10. 29-year average snowmelt (~~a~~A) onset, (~~b~~B) end, and (~~c~~C) period, colored by trend (1987-2016), with bin heights indicating relative number of pixels (i.e. area) at each day of year. Black lines indicate zero trend. Data taken only from areas with statistically significant trends (p <0.05, cf. Fig 9). Changes in snowmelt end date are ~~only~~ positive in ~~a~~ very few ~~, early onset~~ areas. Negative changes in snowmelt period (shortening) are relatively larger in long snowmelt-period areas.

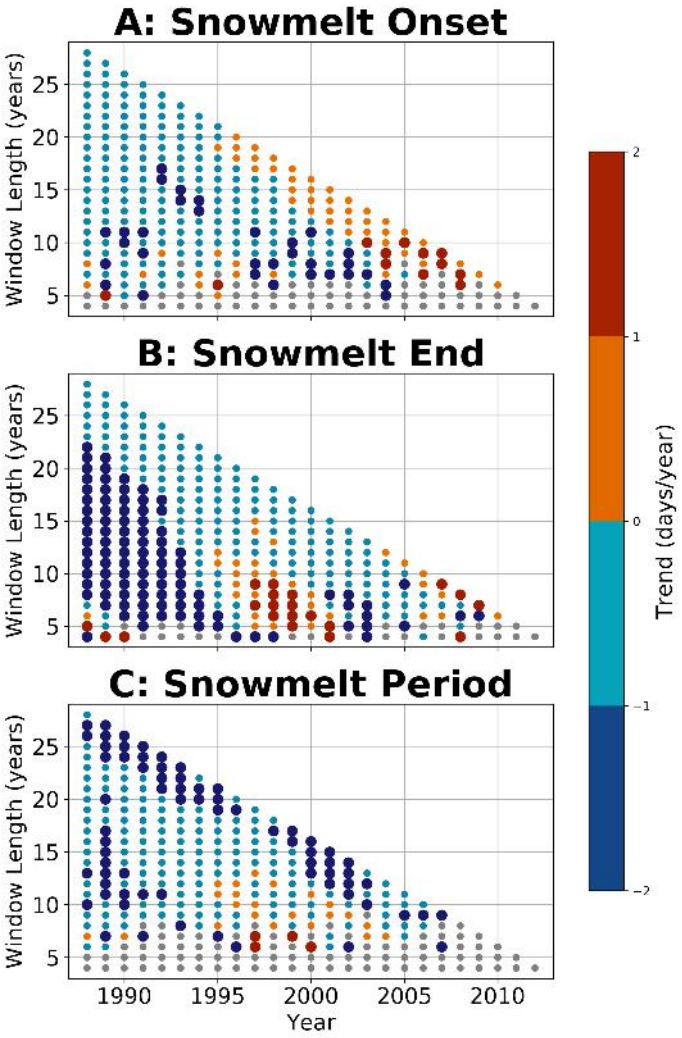

Figure 11. Impact of window length on measured trends in snowmelt (~~a~~A) onset, (~~b~~B) end, and (~~c~~C) period over the entire study area. Each dot represents trends over a single window size (4 to 28 year) and start year (1988-2012) combination. Regressions are performed using the same clusters as shown in Figure 8. Only statistically significant trends (p <0.05) are included in this analysis; gray dots indicate lack of significant trend. Larger dots indicate positive or negative trends larger than 1 day per year. Trends in snowmelt period and snowmelt end dates are ~~almost universally~~ generally negative regardless of which years the trend is assessed over, excepting short periods in the late 1990s and 2000s. Onset dates are positive over short time periods starting in the ~~early 2000s~~late 1990s, and negative over earlier time periods and longer time windows.

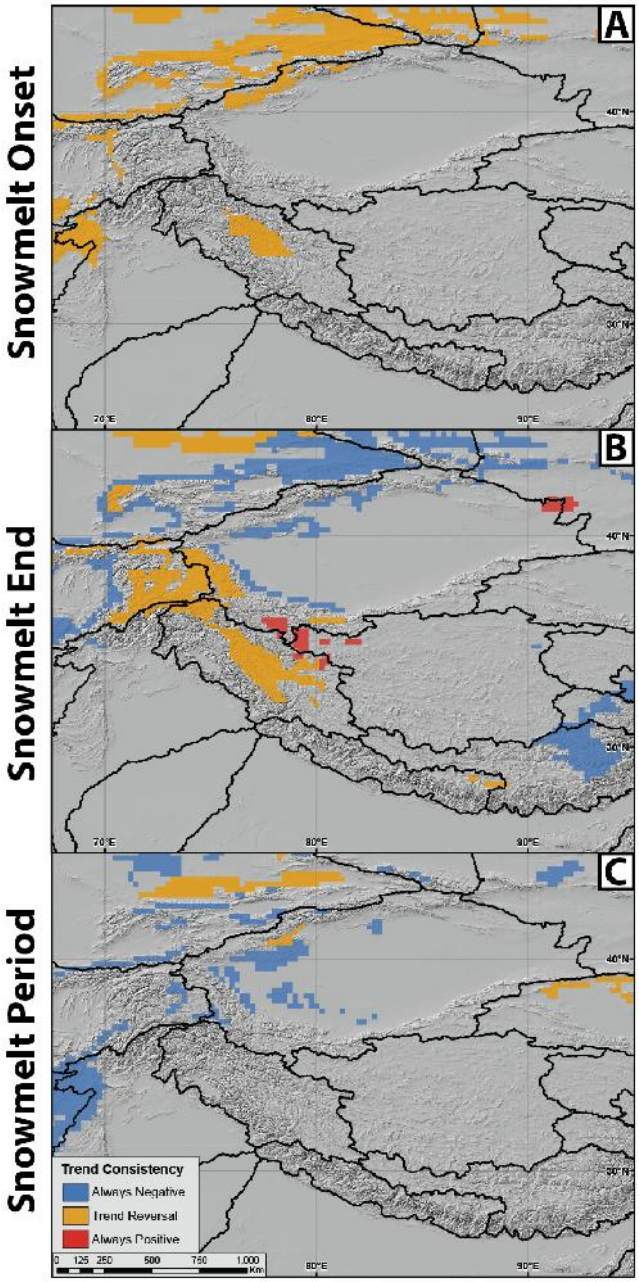

Figure 12. Impact of analysis period (1988-2002 or 2002-2016) on measured trends in snowmelt (~~a~~A) onset, (~~b~~B) end, and (~~c~~C) period. Grey areas indicate lack of statistically significant (p <0.05) trends at one or both analysis periods. Much of HMA lacks significant shorter-term trends in snowmelt onset and snowmelt period, highlighting the complexities and inter-annual variation in snowmelt onset. While ~~much of~~ northern HMA has maintained a negative trend in snowmelt end throughout both analysis timeframes, a large region running from the Pamir east has had a reversed trend from negative to positive in the last decade. Regression results at both individual timeframes are available in the Supplement (Fig. ~~S4~~S8).